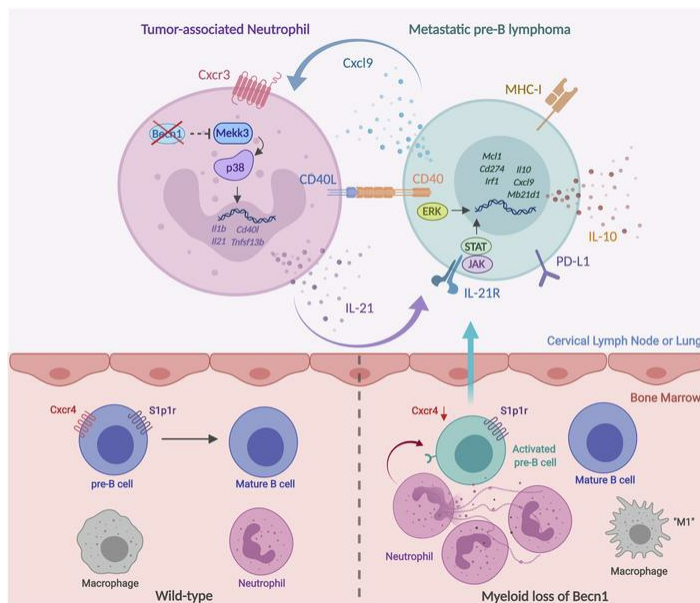# Myeloid loss of *Beclin 1* promotes PD-L1^{hi} precursor B Cell lymphoma development

Peng Tan, … , Helen Y. Wang, Rong-Fu Wang

Research   In-Press Preview   Immunology   Oncology

Graphical abstract

Myeloid Loss of *Beclin 1* Promotes PD-L1[hi] Precursor B Cell Lymphoma Development

Peng Tan,[1,2] Lian He,[2] Changsheng Xing,[1] Jingrong Mao,[1,6] Xiao Yu,[1] Motao Zhu,[1] Lixia Diao,[3] Leng Han,[4] Yubin Zhou,[2] James M. You,[5] Helen Y. Wang,[1] Rong-Fu Wang,[1,2,7] *

[1]Center for Inflammation and Epigenetics, Houston Methodist Research Institute, Houston, TX 77030, USA

[2]Institute of Biosciences and Technology, College of Medicine, Texas A&M University, Houston, TX 77030, USA

[3]Department of Bioinformatics and Computational Biology, The University of Texas MD Anderson Cancer Center, Houston 77030, TX, USA

[4]Department of Biochemistry and Molecular Biology, The University of Texas Health Science Center at Houston McGovern Medical School, Houston, TX, 77030

[5]Department of Hematopathology, The University of Texas MD Anderson Cancer Center, Houston, TX 77030, USA

[6]Xiangya Hospital, Central South University, Changsha 410008, P.R.China

[7]Department of Microbiology and Immunology, Weill Cornell Medical College, Cornell University, New York, NY 10065, USA

*Address correspondence to Rong-Fu Wang, 6670 Bertner Ave, R9-460, Houston, TX 77030. Email: rwang3@houstonmethodist.org; Tel: +1 (713)441-7359

Conflict of interests: The authors have declared that no conflict of interest exists.

Keywords: pre-B ALL; myeloid cells; Beclin 1; neutrophil; inflammation; neutrophil extracellular trap; p38 signaling; IL-21; PD-L1

ABSTRACT

Beclin 1 (Becn1) is a key molecule in the autophagy pathway and has been implicated in cancer development. Due to the embryonic lethality of homozygous Becn1-deficient mice, the precise mechanisms and cell-type-specific roles of Becn1 in regulating inflammation and cancer immunity remain elusive. Here, we report that myeloid-deficient *Becn1* (*Becn1*$^{\Delta M}$) mice developed neutrophilia and were hypersusceptible to LPS-induced septic shock, and had a high risk of developing spontaneous precursor (pre)-B cell lymphoma with elevated expressions of immunosuppressive molecules programmed death ligand 1 (PD-L1) and IL-10. *Becn1* deficiency resulted in the stabilization of MEKK3 and aberrant p38 activation in neutrophils, and mediated the neutrophil-B cell interaction through Cxcl9/Cxcr3 chemotaxis. Neutrophil-B cell interplay further led to the activations of IL-21/STAT3/IRF1 and CD40L/ERK signaling, PD-L1 expression, and thus suppressed CD8$^+$ T cell function. Ablation of p38 in *Becn1*$^{\Delta M}$ mice prevented neutrophil-inflammation and B cell tumorigenesis. Importantly, the low expression of Becn1 in human neutrophils was significantly correlated with the PD-L1 levels in pre-B acute lymphoblastic lymphoma (ALL) patients. Altogether, our findings have identified myeloid Becn1 as a key regulator of cancer immunity and therapeutic target for pre-B lymphomas.

INTRODUCTION

Autophagy has been well recognized as a key intracellular degradation and recycling machinery for maintaining the cellular homeostasis, whose dysregulation leads to cancer (1). Beclin1 (Becn1) acts as a core component of the class III phosphatidylinositol 3-kinase Vps34 complex, which is critical for the initiation of autophagy and autophagosome formation (2). Becn1 is firstly described as a tumor suppressor, as monoallelic deletion of *Becn1* results in spontaneous tumor formation (3). However, given the complexity of the tumor microenvironment, which requires the spatiotemporal interactions between tumor cells and other non-tumor components such as fibroblast, stroma, endothelial and myeloid cells, the cell-type-specific roles of Becn1 in tumor development and immunity are still elusive. Neutrophil is an important component in cancer immunity (4), and regulates many other diseases such as Alzheimer's disease (5) through the release of cytokine IL-21, IL-17, and neutrophils extracellular traps (NETs). For instance, neutrophils with B cell helper phenotype are correlated with tumor development (6-8). However, the detailed mechanism that controls the neutrophil differentiation toward a pro-tumorigenic B cell helper phenotype is undefined.

Cancer cells escape from T-cell-mediated cytotoxicity by exploiting the inhibitory immune checkpoint molecules, including the receptor of programmed death-1 (PD-1) and its ligand PD-L1. Binding of PD-L1 to its receptor PD-1 on activated T cells inhibits the T cell-activating signals and antitumor immunity (9). Notably, B-cell lymphomas also leverage the PD-L1/PD-1 checkpoint to induce the immune escape (10). PD-L1 expression in cancer cells is regulated by mechanisms including aberrant oncogenic and inflammatory signaling and protein stability (9). However, mechanisms regarding the

recruitment of specific myeloid subsets to interact with cancer cells, and drive the tumor development and immune evasion through immune checkpoint molecules, are still elusive.

In this study, we show that neutrophil-derived inflammation is critical for the mice survival to LPS-induced septic shock and responsible for the high incidence (~25%) of spontaneous pre-B cell lymphoma development in mice with myeloid-specific ablation of *Becn1*. We further identify Becn1 as a neutrophil-specific negative regulator of MEKK3-p38 signaling axis in an autophagy-independent manner, which is critical for 1) the expressions of B cell pro-survival factors IL-17, IL-21, and BAFF; 2) the interaction of neutrophils and B cells through CXCR3/CXCL9 chemotaxis; 3) persistent activation of IL-21/STAT3-IRF1 and CD40L/ERK signaling in B cells that together regulate PD-L1 expression to suppress the anti-tumor CD8$^+$ T cell function. Consistently, by analyzing the human pre-B acute lymphoblastic lymphoma patient samples, we reveal that the low expression of Becn1 in tumor-infiltrated neutrophils correlates with tumor PD-L1 expression, and significant positive correlations are also observed between any two of the following three factors: neutrophil marker, IL-21, and PD-L1. Altogether, our findings identify myeloid Becn1 as a non-cell-autonomous tumor suppressor in the regulation of pre-B cell malignancy and immunosuppressive function.

RESULTS

Myeloid-specific Ablation of *Becn1* Induces Splenomegaly and Lymphadenopathy with Neutrophilia

To investigate the role of Becn1 in myeloid lineage development and innate immune response, we crossed *Becn1^{flox}* mice with mice expressing the lysozyme promoter-driven *Cre* recombinase gene (*Lyz2-Cre*), designated as *Becn1$^{\Delta M}$* mice. Co-housed littermate

4

Becn1[WT] or *Becn1*[flox];Lyz2-Cre^{-} mice were used as WT controls. Conditional *Becn1* deletions in F4/80^{+}CD11b^{+} peritoneal macrophages (pMAC) and Ly6G^{+}CD11b^{+} neutrophils were verified by immunoblot analyses compared to CD11c^{+} conventional dendritic cells (cDCs), CD4^{+} T cells, and CD19^{+} B cells (**Supplemental Figure 1A**). Notably, *Becn1*[ΔM] mice developed splenomegaly and had profound enlargements on inguinal, axillary and mesenteric lymph nodes (LNs) (**Figure 1, A and B**). Spleen mass and the total number of splenocytes were markedly increased (**Figure 1A and Supplemental Figure 1B**). Histological analysis of spleen sections revealed a marked effacement of the splenic architecture with loss of marginal zone barriers and a concomitant loss of the clear-cut delimitation between the lymphoid and myeloid parenchyma (**Figure 1A,** bottom). Hematologic analysis of peripheral blood in *Becn1*[ΔM] mice showed increased circulating neutrophils, white blood cells, and eosinophils, but decreased platelets (**Supplemental Table 1**). Consistently, expanded Ly6G^{+} splenic neutrophils with normal shape and segmentation accumulated in the red pulp of spleen surrounding marginal zone (MZ) B cells (**Supplemental Figure 1C**).

Loss of myeloid-specific *Becn1* markedly increased the number of Gr-1^{+}CD11b^{+} myeloid-lineage cells, which is mainly contributed by the increase of Ly6G^{+}CD11b^{+} neutrophils in the bone marrow (BM) and spleen (SP). However, the percentage of F4/80^{+}CD11b^{+} macrophages and CD11b^{+}Ly6C^{+} monocytic cells remained unchanged (**Figure 1, C-G**). Besides, we found an increase in total spleen B220^{+} B cells in some of the *Becn1*[ΔM] mice (**Figure 1C**), but not B220^{+}CD11c^{+}CD11b^{-} plasmacytoid dendritic cells (pDCs) (**Supplemental Figure 1D**). There was no significant difference in the percentage of different CD4^{+} T cell subsets and T cell functions for cytokine release (**Supplemental**

Figure 1, E and F). Gr-1$^+$CD11b$^+$ cells and F4/80$^+$CD11b$^+$ cells also showed equal levels of apoptosis (**Supplemental Figure 1G**). We further transplanted a 1:1 mixture of CD45.1$^+$ wild-type (WT) and *Becn1*$^{\Delta M}$ CD45.2$^+$ BMs into lethally irradiated CD45.1$^+$ WT mice, in which *Becn1*$^{\Delta M}$ CD45.2$^+$ BM cells showed a growth advantage (**Supplemental Figure 1H**). The neutrophil counts of mice reconstituted with *Becn1*$^{\Delta M}$ CD45.2$^+$ BM cells were approximately 4-fold higher than those that received CD45.2$^+$ WT BM (**Supplemental Figure 1I**). Together, our results suggest that neutrophilia in *Becn1*$^{\Delta M}$ mice is driven by factors intrinsic to hematopoietic cells, causing accelerated proliferation and/or enhanced survival of neutrophil progenitors or mature neutrophils.

Becn1 Negatively Regulates p38 Activation and Inflammation in Neutrophils

We next examined TLR-mediated innate immune signaling responses between WT and *Becn1*-deficient neutrophils and macrophages in the periphery of 6- to 8-week-old mice, and found that p38 MAPK activity was increased, while IKK activation was slightly reduced in neutrophils after LPS (a TLR4 ligand) or Pam3CSK4 (a TLR2 ligand) stimulation (**Figure 2, A and B, and Supplemental Figure 2, A and B**). *Becn1*-deficient neutrophils produced a higher amount of TNF-α and IL-1β, whereas *Becn1*-deficient macrophages produced higher amounts of TNF-α and IL-6 (**Figure 2C**). Consistently, we observed an increase in the expression of pro-IL-1β in *Becn1*-deficient neutrophils, but not in macrophages (**Figure 2D**). It has been shown that significant accumulation of neutrophils in the model of *Listeria*-infected *SRB1*$^{-/-}$ mice compared to WT mice, suggesting a critical role of SR-B1 in the differential regulation of neutrophils and macrophages (11). However, no difference was observed in *Scarb1* expression in *Becn1-*

deficient neutrophils and macrophages with or without LPS treatment (**Supplemental Figure 2C**). Therefore, the differential regulation of Becn1 in the activation of p38 and proinflammatory cytokine production is cell-type-specific but independent of SR-B1.

Also, Becn1 expression was induced during "M2 macrophage" polarization by IL-4 or IL-10 (**Supplemental Figure 2D**). *Becn1*-deficient bone-marrow macrophages were readily differentiated to pro-inflammatory "M1 macrophages" by LPS (**Supplemental Figure 2E**). To further define the physiological function of Becn1, we showed that *Becn1*$^{\Delta M}$ mice died after LPS-induced endotoxin shock (30 mg/kg) within 12 h, compared with WT mice that survived for up to 40 h (**Figure 2E**). Consistent with this observation, *Becn1*$^{\Delta M}$ mice had markedly elevated serum concentrations of proinflammatory cytokines such as TNF-α, IL-6, and IL-1β after LPS treatment (**Figure 2F**). Since reactive oxygen species (ROS) are closely linked to inflammation (12), we treated neutrophils and macrophages with LPS for 180 min and then incubated cells with CM-H2DCFDA for 30 min. Flow cytometry analysis revealed a modest increase of ROS production in *Becn1*-deficient neutrophils (**Supplemental Figure 2F, upper panel**). In contrast, ROS production was lower in *Becn1*-deficient macrophages than in WT cells after LPS stimulation (**Supplemental Figure 2F, lower panel**). To determine which cell type contributed to the susceptibility of *Becn1*$^{\Delta M}$ mice to LPS treatment, we depleted macrophages using clodronate-containing liposomes (13) and neutrophils using Ly6G antibody (IA8) (14) (**Supplemental Figure 2G**). We found that macrophage depletion did not change the mouse survival after LPS-induced septic shock. However, there was a significantly prolonged survival in neutrophil-depleted mice (**Figure 2G**), indicating that neutrophils play a dominant role in LPS-induced septic shock. These results suggest that

Becn1 deletion in myeloid cells enhances the sensitivity and severity of LPS-induced septic shock, probably through the increased serum concentrations of proinflammatory cytokines.

To determine the role of Becn1 in regulating the innate immune signaling and gene expression in neutrophils, we performed an RNA-seq analysis of freshly isolated neutrophils with 4h LPS treatment. Interestingly, we observed marked upregulation of genes involved in pathways related to inflammation, rheumatoid arthritis and inflammatory bowel diseases (**Figure 2H, Supplemental Figure 2H and Supplemental Table 2**). The key candidates included genes encoding IL-17 and related cytokines, chemokine receptor and chemotaxis, cell metabolism, and immunity. Neutrophils are another source of IL-17 besides Th17 cells (5, 15-17). We next isolated *Becn1*-deficient neutrophils and peritoneal macrophages and treated them with LPS, and found significantly higher levels of IL-17A and IL-21 in *Becn1*-deficient neutrophils, compared with WT controls or macrophages (**Supplemental Figure 2I**). Together, our results suggest that *Becn1* deletion enhances p38 activation and produces large amounts of IL-1β, TNF-α, IL-17, and IL-21 in neutrophils.

Autophagy-Independent Degradation of MEKK3 by Becn1 Suppresses p38 Signaling

Since NF-κB and MAPK pathways trigger the downstream signaling of IKK complex, Erk1/2, p38, and JNK through the activation of MAP3Ks (TAK1, ASK1, MEKK3) (18), we tested whether Becn1 interacted with these key signaling molecules, and observed strong interaction of Becn1 with MEKK3 and MKK3, only weak interaction with IKKβ and NEMO,

and no interaction with IKKα, ASK1, TAK1 or p38 (**Figure 3, A and B**). Importantly, we found that MEKK3 protein was markedly reduced with an increasing amount of Becn1 in 293T cells (**Figure 3C**). Consistently, we found that the endogenous level of MEKK3 was markedly increased in *Becn1*-deficient neutrophils, but not macrophages (**Figure 3, D and E**). In addition, *Becn1*-deficiency increased the activation of MKK3/6, the MEKK3-downstream mediator for p38 activation (**Figure 3F**). These results suggest that Becn1 regulates MEKK3 stability and MEKK3-p38 signaling activation in neutrophils.

To understand how Becn1 regulates MEKK3 for degradation, we showed that proteasome inhibitor MG132, but not autophagy inhibitors 3-Methyladenine (3-MA) or chloroquine (CQ), blocked Becn1-mediated MEKK3 degradation (**Figure 3G**), suggesting that Becn1 degrades MEKK3 through a proteasome-dependent manner. Protein lysine (K) 48-linked ubiquitination has emerged as an important mechanism to target a protein for proteasomal degradation (19). To identify key lysine residues in MEKK3 required for K48-linked ubiquitination, we substituted a series of lysine residues with arginine and found that lysine 299 (K299) residue was essential in Becn1-mediated MEKK3 ubiquitination and proteasome degradation (**Figure 3, H and I**). These results suggest that Becn1 targets MEKK3 for ubiquitination-dependent proteasomal degradation through K299 residue in MEKK3.

Genetic Ablation of p38 or MEKK3 Rescues *Becn1*ᐧᴹ Mouse Phenotypes

To test whether specific deletion of p38 (encoded by *Mapk14*) or MEKK3 (encoded by *Map3k3*) could rescue the phenotypes and survival in response to LPS-induced septic shock of *Becn1*ᐧᴹ mice, we generated *Mapk14*flox/flox:*Becn1*flox/flox:*Lyz2-Cre* double KO

($Becn1^{\Delta M}$:$Mapk14^{\Delta M}$) mice. Gross phenotypic analysis revealed reduced the spleen size of $Becn1^{\Delta M}$:$Mapk14^{\Delta M}$ that was comparable to WT spleen (**Figure 4A**). Consistently, the extent of CD11b$^+$Gr-1$^+$ cells (41.4% in BM, 14.5% in spleen) of $Becn1^{\Delta M}$ mice was reduced to a level similar to WT mice (22.2% in BM, 7.26% in spleen) in $Becn1^{\Delta M}$:$Mapk14^{\Delta M}$ mice (**Figure 4B**). The serum levels of TNF-α, IL-1β, IL-17 cytokines in $Becn1^{\Delta M}$:$Mapk14^{\Delta M}$ mice were also reduced to the levels similar to WT control, even though IL-6 production remained at a relatively higher level in both $Becn1^{\Delta M}$:$Mapk14^{\Delta M}$ and $Becn1^{\Delta M}$ mice (**Figure 4C**). Importantly, p38 ablation in $Becn1^{\Delta M}$ prolonged the survival to the level similar to WT mice in response to LPS-induced septic shock, but $Becn1^{\Delta M}$:$Il6^{-/-}$ double knockout mice failed to do so (**Figure 4D**), suggesting that TNF-α and IL-1β, but not IL-6, are responsible for the sensitivity to LPS-induced septic shock.

Because mouse $Becn1$ and $Map3k3$ are on the same chromosome (mm11, NC_000077.6), it is difficult to generate $Map3k3^{flox/flox}$:$Becn1^{flox/flox}$:$Lyz2$-Cre double KO mice. For this reason, we used CRISPR-Cas9 genome editing approach (20) to generate $Becn1^{\Delta M}$:$Map3k3^{Cas9}$ BM chimera. BM chimera with WT BM or $Becn1^{\Delta M}$ BM transduced with non-targeting control sgRNA were used as WT or $Becn1^{\Delta M}$ single knockout control. The LPS-induced phosphorylation of p38 in neutrophils isolated from $Becn1^{\Delta M}$:$Map3k3^{Cas9}$ mice was significantly reduced (**Figure 4E**). In addition, neutrophil number and the serum levels of proinflammatory cytokines TNF-α, IL-1β and IL-17 in $Becn1^{\Delta M}$:$Map3k3^{Cas9}$ mice were restored to WT chimeric control (**Figure 4, F and G**). Consistently, $Becn1^{\Delta M}$:$Map3k3^{Cas9}$ mice were more resistant to LPS when compared to $Becn1^{\Delta M}$ group (**Figure 4H**). These results indicate that p38 or MEKK3 ablation in

neutrophils restores inflammatory cytokine (TNF-α, IL-1β, and IL-17) production and reduces the hypersensitivity to LPS-induced septic shock observed in *Becn1*^ΔM mice.

Spontaneous Development of Metastatic Pre-B Cell Lymphoma in *Becn1*^ΔM Mice

During this work, we unexpectedly observed the occurrence of highly proliferative lymphoma in the cervical LNs in 40% of *Becn1*^ΔM mice (**Figure 5, A and B**) with accumulating infiltration of tumor cells in other tissues such as lungs, heart, and thymus (**Supplemental Figure 3A**). Hematoxylin & eosin (H&E) staining of the infiltrated tumor cells revealed that the medium-size tumor cells contained centrally located and prominent nucleoli (**Supplemental Figure 3A**), suggesting a pre-B cell lymphoblastic lymphoma phenotype (21). These tumor cells were positive for B220 staining, but negative for monocyte (Mac-3), macrophage (Mac-1), neutrophil (Ly6G), or T cell (CD3) markers (**Figure 5C,** and **Supplemental Figure 3, B-D**). The B cell-origination of these tumor cells were further confirmed by PAX5 staining in lung infiltrates. Of note, lung-infiltrated tumor cells contained majority the PAX5$^+$B220$^{lo/-}$ cells, but also PAX5$^+$B220$^+$ populations (**Figure 5D)**, when using low B220 antibody concentration (T1 1:500 dilution, vs. high concentration (T2) 1:50 dilution), suggesting the heterogeneity of tumor cells. Unlike the B cell lymphoma in *Becn1*^+/- mice that expresses BCL-6 protein (3), we found that the LN or lung-infiltrated B220$^+$ tumor cells in *Becn1*^ΔM mice were negative for BCL-6 (**Figure 5E**).

Using CFSE (carboxyfluorescein succinimidyl ester) labeling, we showed that B cells isolated from *Becn1*^ΔM tumor-bearing mice were more proliferative than WT B cells after the treatment with LPS and IL-4 (**Figure 5F**). Malignant B cells from *Becn1*^ΔM tumor-bearing mice also displayed a unique phenotype with increased expressions of B cell

surface markers, including CD16/32 [FcYRIII/FcYRIIa], activation marker CD80, CD86, and MHC class I (**Figure 5G**). Importantly, the elevated percentages of pre-B cells expressed low/intermediate B220 (16.8% in tumor vs. 0.78% in WT LN) and pre-B cell marker TdT (**Figure 5, H and I**). These pre-B cells were likely egressed from BM which displayed a loss of pre-B/immature B cells that migrated into secondary lymphoid organs (**Figure 5, J and K, and Supplemental Figure 3E**). We found a small population of autoreactive CD3+/B220+ double-positive cells proliferated in $Becn1^{\Delta M}$ mice, as an autoimmunity-prone phenotype observed in Fas-mutant lpr/lpr lupus mice (22) (**Figure 5H, circled**). Consistently, Giemsa staining of BM cells showed a significant loss of lymphocytes with dark nucleus staining and an increased number of granulocytes (**Supplemental Figure 3F, upper panel**). Further, the cell-cell junction in bone sections of $Becn1^{\Delta M}$ mice was not as tight as in WT mice, as evident from the H&E staining (**Supplemental Figure 3F, lower panel**). Since sphingosine-1-phosphate receptor (S1P1R) or CXCR4 controls B cell BM egression or retention (23, 24), respectively, we sorted B cells from both WT and $Becn1^{\Delta M}$ mice and found a marked reduction of CXCR4 expression, but not S1P1R, in B cells from $Becn1^{\Delta M}$ mice (**Figure 5L**), which might contribute to the pre-B cell BM egression.

***Becn1*-Deficient Neutrophils Interact with B Cells in Tumor Sites**

By using immunohistochemical staining and immunofluorescence, we observed the colocalization of B cells with a large number of neutrophils in the tumor sites, lungs, and intestinal Peyer's patches (with a strip of neutrophils surrounding B cell zone) (**Figure 6, A-C, and Supplemental Figure 4A**). To determine the gene expression profiling of the

tumor and a potential role of neutrophils in the tumor development, we extracted total RNA from cervical LN tumors for RNA-seq, and found many overexpressed genes in *Becn1*$^{\Delta M}$ mice, including those encoding inflammatory and B cell-stimulating molecules (Nos2, Ptgs2, Il21, Il1b, Il12, Tnfsf13b, Tnfsf18, Nlrp3), chemoattractants (Cxcl9, Cxcr3), neutrophil marker (Ly6g), and critical mediators of apoptotic cell removal (**Supplemental Figure 4, B-E, and Supplemental Table 3**). Transcriptional factors Ebf1 and Pax5, which have been reported to essentially contribute to the expansion of B-cell progenitors and acute lymphoid leukemia transformation (25), were also upregulated (**Supplemental Figure 4F**). Notably, the downregulated genes included cell junction molecules related to leukocyte transendothelial migration (Cdh1, Cldn, Tjp1) (**Supplemental Figure 4, B and G**), which might permit the noncanonical interactions between B cells and activated myeloid cells.

Neutrophils have been illustrated to acquire a B-cell helper phenotype to promote B cell expansion and malignancy through several different mechanisms, including 1) contact-independent cytokine secretion such as Tnfsf13b and IL-21, and 2) contact-dependent mechanisms such as CD40 and neutrophil extracellular traps (NETs) (6, 7). Except for MCL-1 and BCL-2, marked upregulation of B-cell helper signature genes was observed in *Becn1*-deficient neutrophils from tumor-bearing mice (**Figure 6, D and E**).

Furthermore, we found an increased accumulation of Ly6G$^+$ neutrophils in the tumor (LN and Lung infiltrates) with auto-activation of p38, which might contribute to IL-21 production (**Figure 6F**). Since myeloid-derived suppressor cells (MDSCs) expressed Gr-1 (Ly6C and/or Ly6G) and CD11b molecules are known to dampen immune response by inhibiting CD4$^+$ and CD8$^+$ T lymphocyte function in cancer, we tested whether the

accumulation of Ly6G⁺CD11b⁺ cells in *Becn1*ᐃᴹ mice have a suppressive function. The T cell proliferation assay (determined by the incorporation of [³H] thymidine) showed that neutrophils (Ly6G⁺) isolated from *Becn1*ᐃᴹ mice (either with or without B cell lymphoma) had no significant suppressive effect on T cell proliferation (**Supplemental Figure 4, H and I**).

Staining of *Becn1*-deficient neutrophils derived from tumor-bearing mice with SYTOX impermeable DNA dye revealed an increased projection of NETs (**Figure 6G**). Thus, the recruitment of neutrophils by B cells through Cxcl9/Cxcr3 chemotaxis (**Figures. 2H, and 6, H and I**) might provide extensive survival signals and inflammatory environment, leading to the malignant transformation of B cells.

Neutrophil with Deficiency of *Becn1* Induces PD-L1 in Pre-B Lymphomas

To determine how the myeloid-specific loss of *Becn1* contributes to the malignancy of B cells, we isolated the total B cells from WT and *Becn1*ᐃᴹ tumor-bearing mice for RNA-seq and real-time PCR analysis. Marked upregulation of different genes were observed, including: 1) STAT target genes such as *Cxcl9*, *Socs1*, *Socs3, Irf1* and *Cd274 (PD-L1)*; 2) precursor B (pre-B) cell markers such as IL2ra and Ly6a (26); 3) B cell activation markers such as IL10 and Saa3; 4) MHC class I related molecules such as Nlrc5 and Psmb9; and 5) innate immunity gene Mb21d1 (cGAS), known to suppress homologous recombination-mediated DNA repair in nucleus and promote tumorigenesis (27) (**Figure 7, A and B, and Supplemental Table 4**).

We next sought to examine whether the tumor cells had altered oncogenic signaling, as suggested in previous studies (28, 29). The tumor and control cells were

sorted by B220 positive selection followed by immediate lysis or anti-CD40 agonist stimulation. We observed elevated activations of ERK and JNK; downstream signaling of IL-21 (p-STAT1, p-STAT3, p-STAT5, with total STAT3 unchanged); and BAFF (non-canonical NF-κB p52); as well as upregulated STAT5-target (anti-apoptotic gene MCL-1) (30) (**Figure 7C and Supplemental Figure 5A**). A recent study demonstrates that hyperactivation of AKT by PTEN ablation triggers the death of pre-B cells (26). However, we did not observe the changes of AKT and FOXO1 phosphorylation in these B cells (**Supplemental Figure 5A**). Consistent with the upregulation of MCL-1, we observed reduced apoptosis of B cells isolated from the tumor but not the non-tumor bearing *Becn1*$^{\Delta M}$ mice (**Supplemental Figures 1G and 5B**). Moreover, we compared the signaling activations in B cells from WT, tumor-free *Becn1*$^{\Delta M}$ (NT), and B220^{hi} vs. B220^{lo} cells from tumor-bearing *Becn1*$^{\Delta M}$ mice, and found that B220^{lo} cells had higher levels of phosphorylated STAT1/3/5 and PD-L1 than B220^{hi} cells (**Figure 7, D and E, circled**). By co-culturing the neutrophils or macrophages from tumor-bearing *Becn1*$^{\Delta M}$ mice with normal WT B cells, we found the induction of PD-L1, as well as CXCR3 ligands Cxcl9/10, in B cells by neutrophil-derived factors (**Supplemental Figure 5, C and D**). Further, the upregulation of PD-L1 could be abolished by antibody blockade of either IL-21 or CD40L (**Supplemental Figure 5E**). To understand the signaling pathways in B cells that control the expression of PD-L1, we applied MAP kinase inhibitors (p38i, SB 203580; ERKi, U0126; JNKi, sp 600125), NF-κB inhibitor (BAY 11-7082), and STAT3 inhibitor (STAT3i, WP 1066) to sorted B cells after co-culture with *Becn1*-deficient neutrophils. The inhibition of ERK and STAT3 could reduce the PD-L1 level, suggesting that both ERK and STAT3 signaling pathways are involved in the regulation of PD-L1 expression (**Supplemental**

Figure 5F). We also detected the upregulation of IRF1 in B cells (**Figure 7, A and B**), which is an essential transcriptional factor-mediated STAT signaling and the expression of both PD-L1 and MHC-I molecules (31, 32). In addition, ERK signaling promotes PD-L1 expression through the negative regulation of TTP (Tristetraprolin, encoded by Zfp36) expression and activity, which is a zinc-finger RNA-binding protein that suppresses PD-L1 mRNA through binding to the AU-rich element at 3'-UTR (33). By inhibition of STAT3 and ERK signaling, we observed reduced levels of Irf1 (by STAT3i) and increased levels of Zfp36 (by ERKi) (**Supplemental Figure 5G**), suggesting that the activations of both ERK-TTP and STAT3-IRF1 signaling by neutrophil-derived factors contributed to the upregulation of PD-L1 expression in pre-B lymphoma cells. Notably, no change was observed in the expression of Cmtm4/6, which stabilize the PD-L1 protein (34), in B cells after co-culture with *Becn1*-deficient neutrophils (**Supplemental Figure 5H)**.

To further demonstrate the effects of neutrophil factors that promote the PD-L1 expression *in vivo*, we treated *Becn1*$^{\Delta M}$ mice (6-to-8-week-old without tumors) by intraperitoneal (i.p.) injection of recombinant neutrophil factors (**Supplemental Figure 6A**) and found that IL-21 significantly promoted the enlargement of cervical LN as well as PD-L1 expression in sorted CD19^{+} or B220^{+} B cells (**Supplemental Figure 6B**). On the contrary, irradiated *Becn1*$^{\Delta M}$ mice reconstituted with bone marrow from tumor-bearing *Becn1*$^{\Delta M}$ mice with IL-21 ablation (*Becn1*$^{\Delta M:}$*Il21* KO) showed a reduction of PD-L1 expression and STAT3 activation (**Figure 7, F and G).** To further examine the physiological role of PD-L1 molecules in cancerous pre-B cells in the regulation of the endogenous anti-lymphoma CD8^{+} T cells, we injected *Becn1*$^{\Delta M}$ tumor-bearing mice with the antibodies against PD-L1 or IL-21R, compared to mice injected with IgG control, and

found a significantly increased number of total CD8$^+$ cells as well as CD8$^+$IFN-γ$^+$ and CD8$^+$Granzyme B$^+$ T cells in the tumor region (**Supplemental Figure 6, C and D**).

Since p38 signaling regulated neutrophil inflammation in *Becn1*^{ΔM} mice in response to TLR ligand stimulation **(Figures 2, 4)**, which was auto-activated in tumor-derived neutrophils (**Figure 6F**), we next examined if ablation of p38 could reduce the expressions of neutrophil-derived B cell activation factors (e.g. IL-12, CD40L, IL-1β, IL-21, and BAFF), immunosuppressive molecule PD-L1, and the risk of B cell lymphoma in *Becn1*^{ΔM} mice. Indeed, myeloid-specific ablation of p38 in *Becn1*^{ΔM} mice restored the expressions of neutrophil-derived B cell activation factors, reduced STAT3 phosphorylation and PD-L1 expression, B cell BM egression, and in turn suppressed the spontaneous tumor development in *Becn1*^{ΔM} mice (**Supplemental Figure 6, E-H)**.

To investigate whether Becn1 in human neutrophils plays a role in human B-cell lymphoid malignancies, we first analyzed Becn1 expression in a series of human B-cell non-Hodgkin lymphomas (B-NHL) and pre-B cell acute lymphoblastic leukemia/lymphoma (ALL, without mutations or gene-rearrangements) by human gene expression profiling (GEP). Becn1 expression levels varied significantly among the different B-cell lymphoid malignancies, with the lowest level in pre-B ALL and highest in MCL and CLL (**Supplemental Figure 6I and Supplemental Table 5**). Furthermore, we found a lower Becn1 expression in neutrophils among human pre-B ALL patients compared to normal controls (**Figure 7H**). Notably, in recurrent pre-B ALL patient, neutrophils with low Becn1 expression had the NET-like structure (**Figure 7H, left panel, recurrent hPre-B ALL**). Consistent with the upregulation of PD-L1 in B cells from *Becn1*^{ΔM} mice, we found upregulation of PD-L1 in pre-B ALL patient BM and LN samples

especially in recurrent pre-B ALL samples (**Figure 7I**). In a clinical study of B-ALL patients (TARGET ALL projects), significant positive correlations were observed in among the expression of IL-21, PD-L1 (CD274), and neutrophil markers (human ortholog LY6G6D and CD177) (35, 36) (**Figure 7J, Supplemental Figure 6J**). These data suggest that low Becn1 expression in neutrophils might have a direct link to the PD-L1 level expression and recurrence in human pre-B ALL. Thus, our results suggest that the low Becn1 expression in neutrophils correlates with the PD-L1 levels in the pre-B ALL patients.

DISCUSSION

Despite the importance of autophagy in macrophages during *Mycobacterium tuberculosis* infection or LC3-associated phagocytosis (37, 38), little is known about the *in vivo* function of Becn1 in neutrophils regarding the inflammation and cancer immunity. Our study showed that deletion of *Becn1* in the myeloid lineage lead to neutrophilia, which caused splenomegaly and lymphadenopathy in mice. We uncovered a cell-type-specific mechanism of Becn1 as a negative regulator of p38 signaling in neutrophils to LPS stimulation. Depletion of neutrophils, but not macrophages, could rescue the sensitivity of *Becn1*$^{\Delta M}$ mice to LPS endotoxin shock, suggesting an excessive LPS-induced neutrophil inflammation. Our cytokine profiling and RNA-seq analyses further revealed the enhanced productions of TNF-α, IL-1β, ROS, IL-17-related cytokines, and chemokine-receptor CXCR3 by neutrophils in *Becn1*$^{\Delta M}$ mice. The p38 MAPK signaling is critical for the transcription and production of inflammatory cytokines (39, 40). Consistent with the cell depletion results, we provided compelling genetic evidence that p38 (encoded by *Mapk14*) ablation in myeloid cells rescued the observed phenotypes and the production

of inflammatory cytokines in $Becn1^{\Delta M}$ mice. NF-κB activation is known to negatively regulate IL-1β secretion in neutrophils in myeloid IKKβ-deficient mice (41). Consistently, we observed the reduced IKK phosphorylation and increased IL-1β secretion upon LPS stimulation in $Becn1$-deficient neutrophils. Despite the elevated production of IL-6 in macrophages, IL-6 ablation failed to rescue the survival of $Becn1^{\Delta M}$ mice to LPS-induced septic shock.

It is known that MAP3Ks (TAK1, ASK1, MEKK3) activation triggers downstream signaling of IKK complex, Erk1/2, p38, and JNK (18). We showed that Becn1 interacted with MEKK3 and MKK3, and promoted the MEKK3 K48 ubiquitination at lysine 299 and subsequent autophagy-independent proteasomal degradation. Due to the low protein level of MEKK3 observed in neutrophils, the activation of p38 in neutrophils is mainly triggered by the upstream molecules other than MEKK3, such as TAK1. The stabilization of MEKK3 upon $Becn1$ deletion thus leads to aberrant activation of neutrophils through MEKK3-MKK3-p38 signaling axis. Consistently, further ablation of MEKK3 significantly prolonged the survival of $Becn1^{\Delta M}$ mice to LPS-induced septic shock.

Heterozygous deletion of $Becn1$ increases the incidence of spontaneous tumors in mice, including diffused large cell b-cell lymphoma (DLBCL) (3), suggesting that Becn1 is a haploinsufficient tumor suppressor. However, it is unclear whether the tumor formation is induced by intrinsic factors or by oncogenic inflammation from non-transformed immune cells in the tumor microenvironment. While the Becn1 expression is intact in pre-B cells, $Becn1^{\Delta M}$ mice showed a high risk of TdT$^+$ pre-B cell lymphoma formation (40% frequency) as early as the age of 15-25 weeks. The accumulation of neutrophils, but not macrophages was found to colocalize and interact with malignant B

cells in tumor sites. It is worth noting that neutrophilia was developed in mice with or without lymphoma, probably due to p38 activation and high level of IL-1β, which could cause the accumulation of neutrophils through IL-1R1 signaling (42). Although Becn1 deficiency in myeloid cells did not alter the number and overall infiltration of macrophages, these macrophages are prone to display M1 phenotypes known to be anti-tumor (43). Furthermore, we found that the pre-B tumor cells were egressed from BM. It has been reported that stromal cells, Bruton's tyrosine kinase, S1P/S1P receptor, CXCL12/CXCR4 signaling cascades, and α4β1-VCAM-1-mediated adhesion could all regulate the B cell migration from BM (7, 44-47). Our data suggest that the BM (a major pool of myeloid cells, such as neutrophils) is a critical location for pre-B cells to be activated by local inflammatory neutrophils in tumor-bearing $Becn1^{\Delta M}$ mice. This unique interaction lead to the egression of pre-B (B220^{lo}) cells from BM (by downregulation of BM retention signal Cxcr4, but not the S1P egression signal), serving as a pre-requisite step for the development of metastatic pre-B cell lymphoma in cervical lymph nodes and lungs. We reason that the IL-21 produced by tumor-associated neutrophils and subsequent STAT3/SOCS3 activation in B cells are the potential mechanisms to control the lodgment of precursor B cells in the BM, as it could downregulate the CXCR4 signaling (48, 49).

Recent studies also identify a unique population of IL-21-secreting neutrophils, termed B cell helper neutrophils, to sustain B cell survival, expansion and malignant transformation (7, 8). IL-21 receptor signaling has been linked to inflammation and autoimmune diseases such as SLE (50). IL-21 also enhances inflammation-associated malignancy (51). However, the potential mechanisms underlying the differentiation and transition of neutrophils to gain "B cell helper" function remain unknown. In this study, we

identified that Becn1 is a key regulator governing the transition of normal neutrophils into pro-tumoric neutrophils with upregulated "B helper" signatures, including IL-21, BAFF, CD40L, and the production of NET. These factors have been shown to activate multiple oncogenic signaling pathways, such as STATs and non-canonical NF-κB that are crucial in initiating oncogene transcription and establishing the tumor pre-metastatic niche (29, 52-54). Therefore, myeloid deficiency of Becn1 provides a unique model for investigating the neutrophil-B cell interaction.

Strikingly, when comparing B220^{lo} with B220^{hi} cell populations, we showed that B220^{lo} cells had higher and persistently activated STAT1, STAT3, STAT5, and non-canonical NF-κB p52, followed by the upregulation of their downstream targets MCL-1, chemokine Cxcl9, and checkpoint inhibitor PD-L1. The interaction with *Becn1*-deficient neutrophils also activated B220^{hi} cells in tumor sites but to a less extent, compared with B220^{lo} cells, suggesting the heterogeneity of these tumor cells. We also demonstrated that CD40L/ERK and IL-21/STAT3-IRF1 were key signaling pathways to govern the expression of PD-L1 in pre-B cells. IL-21 treatment in *Becn1*$^{\Delta M}$ mice promoted the lymphoma formation in cervical LN and PD-L1 expression on B cells. These findings are consistent with the previous report that cytokine IL-21 induces PD-L1 expression in CD19^{+} B cells but not in purified T cells (55). Based on these findings, we propose the feed-forward recruitment of neutrophils by pre-B cells via the CXCL9-CXCR3 chemotaxis to promote the development of immunosuppressive pre-B cell lymphoma. Notably, cGAS acts as a tumor enhancer in the presence of genotoxic or ROS stress, through inhibiting homologous recombination mediated DNA repair. Aberrant upregulation of cGAS transcripts are reported in non-small cell lung carcinomas (27). Similarly, we showed that

21

cGAS mRNA level was upregulated in pre-B tumor cells. The potential association between the upregulation of cGAS in pre-B tumor cells and the malignant transformation of pre-B cells awaits further investigation.

PD-L1 is one of the critical checkpoint inhibitory signaling molecules utilized by tumor cells or other immune suppressor cells to inhibit T cell function for immune evasion (56). The PD-L1-expressing IgA$^+$ B cells have been shown to suppress CD8$^+$ T cells to kill liver tumor in a mouse model of inflammation-induced liver cancer (57). Administration of PD-L1 or IL-21R antibody in $Becn1^{\Delta M}$ tumor-bearing mice reversed the suppressive function of immunosuppressive PD-L1^{hi} pre-B cells against CD8$^+$ T cells. Injection of IL-21 increased the risk of developing lymphoma with upregulated PD-L1 in $Becn1^{\Delta M}$ mice, suggesting the critical role of IL-21 in tumor immunity. Importantly, low Becn1 expression in tumor-infiltrated neutrophils correlates with PD-L1 levels in recurrent pre-B ALL patients. In addition, significant positive correlations were observed in pre-B ALL patients between any two of the three factors: neutrophil marker Ly6g, IL-21, and PD-L1, which recapitulates the malignant pre-B cells identified in $Becn1^{\Delta M}$ mice. Together these findings indicate the potential of novel immunotherapy for the treatment of metastatic and/or recurrent pre-B ALL by combining PD-L1 or IL-21 antibody blockade with inhibitors targeting tumor-infiltrating neutrophils. We also offer new evidences to support the critical role of neutrophil-mediated inflammation in the B cell migration and lymphomagenesis. Overall, our results provide molecular insights into the mechanisms of how $Becn1$-deficient neutrophils produce proinflammatory cytokines through regulation of p38 and MEKK3 signaling pathways and promote tumor development by inducing PD-L1

expression in pre-B cells. Thus, myeloid Becn1 may serve as a therapeutic target for cancer immunotherapy.

METHODS

Animals and in vivo procedures. Adult C57BL/6 (CD45.2) and Boy/J (CD45.1) mice were obtained from the Jackson Laboratory. *Becn1*^{flox} mice (Knockout Mouse Project Repository [KOMP]) were crossed with lysozyme-Cre (Lyz2-Cre) mice (Jackson Laboratory) to obtain *Becn1*$^{\Delta M}$ mice on the C57BL/6 background. Mouse genotyping primers to detect WT and flox/flox mutant were as follows: 1) Becn1-1R: 5'-GCGGATCCCTGAGTTCTAGACTAACC-3'; 2) Becn1-1F (ttR): CTCCCAATGCTGGGATTAAAGACG-3'; and 3) Becn1-2R (F): TTGTACCGTGATTTAGGGCGTTTGC-3'. *Becn1*$^{\Delta M}$ mice were bred with *Mapk14*^{flox} mice (provided by Y. Wang, UCLA, and H. Jiang, Boehringer-Ingelheim) or *Il6*$^{-/-}$ mice (Jackson Laboratory) to generate *Becn1*$^{\Delta M}$:*Mapk14*$^{\Delta M}$ and *Becn1*$^{\Delta M}$:*Il6*$^{-/-}$ mice, respectively. To generate *Becn1* and *Map3k3*, *Becn1* and *Il21* double knockout BM chimeric mice, deletions of *Map3k3* and *Il21* were achieved by the clustered regularly interspaced short palindromic repeats (CRISPR)-Cas9 system (20). We used the following single-guide (sg) RNA sequences to target exon1 of *Map3k3*: ACCGGGTTCGTCGGCTCATC and exon1 of *Il21*: *Il21*-sg-RNA-1 GGTGACGAAGTCTAATCAGG and *Il21*-sg-RNA-2 GCTGTTCAACAATGTCAATA. Scrambled mouse sgRNA served as control: GCGAGGTATTCGGCTCCGCG. Total BM was isolated from the femur and tibia of 6 to 10-week-old female C57BL/6 wild-type mice or *Becn1*$^{\Delta M}$ mice. BM was subjected to erythrocyte lysis (BD PharmLyse, BD Bioscience), followed by magnetic bead selection

of cKit-positive cells using CD117 MicroBeads (Miltenyi Biotec). Prior to flow sorting using BD FACSAria II, CD117-selected cells were stained with APC-labeled cKit (eBioscience), PE-labeled Sca1 (BioLegend), PacificBlue-labeled Gr1, CD11b, B220 (CD45R), Ter119, and CD3 (eBiosciences). LSK cells were cultured in StemPro®-34 SFM complete medium (ThermoFisher) supplemented with 50 ng/ml murine Thpo and 50 ng murine Scf (Life Technologies) for 48 h and then transduced with concentrated lentiviral supernatant in presence of 2 µg/ml Polybrene. 24 h post-transduction cells were collected and intravenously injected into lethally irradiated (950 cGy) 6 to 10-week-old female C57BL/6 mice (Jackson Laboratory). Since the CRISPR-Cas9 genotyping data provided only a 'snapshot' of the polyclonal cell population genotype, the possibility that not all alleles had been targeted by this approach could not be ruled out. For BM chimeras, approximately 1.5 x 10^6 total BM cells from CD45.1$^+$ donors (see in Supplemental Table 7) were mixed with 1.5 x 10^6 total BM cells from adult WT (CD45.2$^+$) or *Becn1*$^{\Delta M}$ (CD45.2$^+$) mice and then were transferred into adult WT CD45.1$^+$ mice that had been exposed to 950 cGy. Chimeras were analyzed at least 6 weeks after reconstitution. To study *in vivo* endotoxicity, mice received i.p. injection of LPS (25–30 mg/kg), and blood samples were collected to assay plasma cytokine concentrations.

RNA-sequencing. Total RNA was used for mRNA isolation and cDNA library generation with miRNeasy micro Kit (Qiagen). On-column DNase digestion (DNase-Free DNase Set, Qiagen) was performed according to manufacturer protocols to prevent genomic DNA contamination. RNA and library preparation integrity was verified using a 2100 BioAnalyzer system (Agilent). Ribosomal RNA depletion was performed following the low

input protocol by RiboMinus Eukaryote System v2 (ThermoFisher) with 500 ng total RNA input. Finally, libraries were prepared using the Ion Total RNA-Seq Kit v2 (ThermoFisher) with minor changes to the standard protocol. These included lower amplification cycles and the usage of entire fragmented RNA for cDNA synthesis. For the sequencing reactions, an Ion Torrent Proton platform with V3 chemistry (Ion PI Template OT2 200 Kit v3, ThermoFisher) and PIV2 Chips (Ion PI™ Chip Kit v2, ThermoFisher) were used. The experiment was performed on two chips containing two biological replicates per condition (wt1/mt1 on chip A and wt2/mt2 on chip B) resulting in 163 million total reads and at least 40 million reads per library. Base-calling was performed on Ion Torrent suite software. Raw sequencing reads in FASTQ format were aligned to the UCSC mouse reference genome (mm10) using TOPHAT21 (58). Differentially expressed genes were identified using DESeq2 version 1.62. Only genes with a minimum log2 fold change of +/− 2, a maximum Benjamini-Hochberg corrected p-value of 0.05, and a minimum combined mean of 5 reads were classified as having significant differential expression. Gene set enrichment analysis (GSEA) software was used to perform GSEA against the GSEA database was used (59). The DAVID/EASE software (https://david.ncifcrf.gov/summary.jsp) was used to establish whether specific cell functions and biologic processes, defined according to gene ontology, were significantly represented among the deregulated genes. Data were also analyzed with Ingenuity Pathway Analysis (IPA) software (Ingenuity Systems, www.ingenuity.com). See Supplemental Tables 2-4.

Isolation of Immune Cells. BM cells were isolated from the tibia and femur and cultured in RPMI1640 medium with 10% FBS, 1% penicillin-streptomycin, 55 mM β-mercaptoethanol, and 10% L929 conditioned media containing macrophage-colony stimulating factor for 5 days for BM-derived macrophages (BMDMs), 20 ng/mL murine GM-CSF and 10 ng/ml IL-4 for 6–8 days for conventional DCs. Peritoneal macrophages were obtained by injecting mice i.p. with 3 ml 4% (v/v) thioglycollate (Beckton Dickson) and peritoneal cavities were flushed after 3 days with RPMI 1640 media with 2% FBS. Mouse CD4 cells were isolated from SP or LN by using Dynabeads® untouched mouse CD4 cells kit (ThermoFisher). 10^8 cells/mL of splenocytes and LN cells were blocked with heat-inactivated FBS and antibody mix against CD8, B220, CD11b, Ter-119, and CD16/32. After 20 min incubation at 4°C, cells were washed with isolation buffer (PBS (Ca^{2+} and Mg^{2+} free) supplemented with 0.1% BSA and 2 mM EDTA) and incubated with pre-washed mouse depletion dynabeads for 15min at room temperature (RT). Resuspended beads-bound cells by gently pipetting were placed in the magnet for 2min. Untouched CD4$^+$ T cells in the supernatant were then collected. Similarly, total B cells were isolated from the tumor, LN, SP or BM by using mouse CD45R (B220) microbeads (Mitenyi Biotec) or PE-positive selection beads with PE-B220 antibody. In some experiments, B cells were pretreated with 1 µg/mL CD40L or anti-CD40 (CD40 agonist), 10ng/mL IL-4, 100ng/mL LPS, specific inhibitor of JNK (SP 600125, 5µmol/L), ERK (U0126, 20µmol/L), NFκB (BAY 11-7082, 5µmol/L), p38 (SB 203580, 20µmol/L), STAT3 (WP1066, 5µmol/L). Peripheral neutrophils were obtained from the peritoneal cavity by i.p. injection of mice with 2 ml 4% (v/v) thioglycollate for 4 h followed by the collection of peritoneal exudates with RPMI 1640 media with 2% FBS. Neutrophils were then purified

by sorting Ly6G$^+$CD11b$^+$ cells or using EasySep Mouse Neutrophil Enrichment Kit (Stem Cell Technologies) to remove non-neutrophil populations. Tissue infiltrated neutrophils were purified from intraparenchymal pulmonary or LN cell suspensions using a similar isolation method as peritoneal neutrophils. Briefly, for lung neutrophil isolation, the chest of the mouse was opened, and the lung vascular bed was flushed with 2–3 ml of pre-chilled PBS injected into the right ventricle. Lungs were excised to avoid the paratracheal LNs and thymus and washed twice in RPMI 1640 media supplemented with penicillin/streptomycin. The excised lungs were minced finely, and the tissue pieces were placed in RPMI 1640 medium containing 2% FBS, 20 U/ml collagenase, and 1 g/ml DNase. Following incubation for 60 min at 37°C, any remaining intact tissue was disrupted by passage through a 21-gauge needle. Tissue fragments and the majority of dead cells were removed by rapid filtration through a glass-wool column, and cells were collected by centrifugation. Cells were subjected to the enrichment using EasySep Mouse Neutrophil Enrichment Kit.

Immunoprecipitation and Immunoblot Analyses. For immunoprecipitation, whole-cell lysates were incubated overnight with indicated antibodies plus protein A and G beads (Pierce). For immunoprecipitation with anti-FLAG, anti-FLAG agarose gels were used. Beads were then washed five times with low-salt lysis buffer (50mM HEPES,15mM NaCl, 1mM EDTA, 1.5mM MgCl2, 10% Glycerol, 1% Triton X-100), and immunoprecipitates were eluted with 4 x SDS loading buffer. Immunoblotting was performed by resolving protein lysates on SDS-PAGE gels, followed by transfer to nitrocellulose membranes (Bio-Rad), and further incubating membranes with indicated antibodies overnight (see

Supplemental Table 7). For all blots, EMD Millipore Luminata Western HRP Chemiluminescence Substrate was used for protein detection.

Flow Cytometry. Single-cell suspensions were obtained from tissues and stained for 30 min with indicated antibodies. For intracellular staining, $CD4^+$ or $CD8^+$ T cells were stimulated with PMA (15 nM) and ionomycin (0.5 µM) for 6 hr at 37°C in the presence of GolgiStop (monensin) (BD Pharmingen). Cells were then stained with the surface marker (see Supplemental Table 7) for 15 min on ice and permeabilized using cytofix/cytoperm (BD Biosciences) for 30 min on ice. Permeabilized cells were resuspended in BD Perm/Wash buffer (BD Biosciences) and stained with cytokine antibody for 20 min. FACS analysis was performed with BD LSRII Flow Cytometer (Becton Dickson) and data were analyzed by BD FACSDiva software.

Cytokine Release Assay. Cell supernatants or sera were collected at indicated time points after stimulation with LPS with or without ATP. Cytokine concentrations were determined by ELISA with TNF-α, IL-6, IL-1β, IL-17A, IL-17F, IL-21, IL-22, and BAFF antibodies (See Supplemental Table 7). ELISAs were performed according to the manufacturer's instructions. In brief, 96-well plate was pre-coated with the capture antibody (1:500 in coating buffer) at 4°C overnight. On the next day, the plate was washed with PBS/0.1%Tween 20 and blocked with 1%BSA/PBS diluent buffer for 2 h at RT. Diluted supernatants and cytokine standards were then applied to the plate and incubated for 2 h at RT. The plate was then washed and incubated with biotin-conjugated detection antibody (1:1000 in 1%BSA/PBS diluent buffer) for 1 h at RT. The plate was then washed

28

and incubated with poly-HRP streptavidin (1:5000 in the diluent buffer, Thermo Scientific) for 30 min. The plate was washed again and finally incubated with the tetramethylbenzidine substrate solution (Sigma-Aldrich). The reaction was stopped using 2 M H_2SO_4. The absorbance of each well was recorded by Synergy™ 2 plate reader (Biotek) at 450nm. The absorbance of the standard sample was used to construct the standard curve.

Hematological and Histological Analysis. Complete peripheral blood counts were performed with an automated hematology analyzer (Hemavet 850; Drew Scientific). For whole BM sections, specimens were decalcified in (8%) hydrochloric acid/ (8%) formic acid working solution overnight, followed by neutralization by ammonia solution for 30 min and embedded in paraffin. Embedded BM blocks were sliced and stained with H&E for conventional morphological assessment. For cytocentrifugation preparations, BM cells were subjected to red blood lysis in ACK buffer (0.15 mM NH_4Cl, 1 mM $KHCO_3$, and 0.1 mM Na_2EDTA). Between 2 - 5 × 10^5 cells were suspended in 100 µl PBS, loaded onto disposable Cytofunnel chambers, and centrifuged for 4 min at 400 RPM using a CytoSpin III cytocentrifuge (Shandon). For May-Grünwald Giemsa stain, cytocentrifuged samples were stained in May-Grünwald solution (MG500; Sigma-Aldrich) for 2 min and Giemsa (GS500, 5% solution in water; Sigma-Aldrich) for 12 min, followed by two washes in distilled water for 30 s. Thereafter, samples were cytocentrifuged, counterstained with May-Grünwald solution for 10 s and washed in water. Slides were coverslipped using Permount and analyzed by brightfield microscopy. Immunohistochemical (IHC) staining was performed using the streptavidin-biotin-peroxidase complex method using the

Vectastain Elite ABC kit and DAB peroxidase (HRP) substrate kit. Primary antibodies used were listed in Supplemental Table 7. Negative control staining was performed using mouse, rabbit, or rat immune sera instead of the primary antibodies. Sections of human B cell lymphoblastic leukemia/lymphoma tissues were obtained from Dr. James You (UT MD Anderson Cancer Center, Houston, TX), including 10 pre-B ALLs in LN or BM, and 6 reactive LNs or BM controls. Immunofluorescence (IF) assays and confocal microscopy were conducted using fluorescent secondary antibodies (see Supplemental Table 7). Samples were visualized using Nikon Eclipse Ti-E microscope. All acquired images were analyzed using the Nikon NIS-Elements AR package or the ImageJ (NIH) software.

In vivo Cell Depletion and Antibody Blockade. Monocyte or macrophage depletion was performed by intravenous (i.v.) injection of 250 µl clodronate-containing liposomes (Encapsula NanoSciences) on day -1 relative to LPS treatment. Control liposomes were used as PBS control. Neutrophil/granulocyte depletion was induced with combined 0.5 mg of anti-Ly6G mAb clone 1A8 (BioXcell) or with PBS controls i.p. injection into mice on days -3, -2, and -1 relative to LPS treatment. FACS-sorted B220$^+$ cells were left untreated or were co-cultured with isolated neutrophils in the presence or absence of 10µg/mL antibody against IL-21, BAFF, IFN-γ, IL-1β, or CD40L.

Quantitative RT-PCR (qRT-PCR) Analysis. Total RNA was isolated from cells using RNeasy RNA isolation kit (QIAGEN) and reverse transcribed using SuperScript III Reverse Transcriptase (Invitrogen) as per manufacturer's directions. Quantitative PCR was conducted on the ABI Prism 7000 analyzer (Applied Biosystems) using SYBR

GreenER qPCR Super Mix Universal (Invitrogen). mRNA levels were normalized to Gapdh and relative levels were determined using the ΔΔct method. Primers are listed in Supplemental Table 6.

ROS Measurement and H₂O₂ Treatment. Neutrophils were stimulated with LPS (100 ng/ml) for 0, 10, 30 min, and 3 h at 37°C. Cells were then incubated with or without CM-H2DCFDA (10 μM) in PBS for 30 min at 37°C and analyzed by flow cytometry using FITC channel.

Proliferation and apoptosis assays. Annexin V and 7AAD/PI staining kit (BD Biosciences) was used to detect apoptotic cells following the manufacturer's instructions. T cell proliferation was assessed using [^{3}H] thymidine assay using irradiated neutrophils as antigen-presenting cells (APCs). Briefly, T cells (1 x 10^5) were isolated from spleens and co-cultured with irradiated Ly6G$^+$ CD11b$^+$ cells (2 x 10^5) with the anti-CD3 antibody for 56 h in 96 well plates. T cell proliferation was determined by labeling cultured cells with [^{3}H] thymidine for 16 h and radioactivity was measured using a scintillation counter. Carboxyfluorescein diacetate, succinimidyl ester (CFSE) staining was performed by labeling B cells (1x10^6) with CFSE (5 μM) for 10 min. Cells were washed with PBS, plated in RPMI media containing 10% FBS and 1% (volume/volume) penicillin-streptomycin supplemented with LPS (100 ng/ml) and IL-4 (50 ng/ml) and incubated at 37 °C until they were analyzed by flow cytometry.

GEP of Human Lymphomas. Gene expression analysis was performed on datasets from Gene Expression Omnibus (GEO, https://www.ncbi.nlm.nih.gov/geo/) including GSE12195, GSE26673, GSE16455, GSE12195, GSE16455, GSE7440, GSE11877. Specifically, we included the following cancer types: 16 BL, 18 CLL, 38 FL, 75 DLBCL, 22 MCL, 4 MZL, 306 B-ALL, and 5 naïve cell samples. Data were processed by Affymetrix Expression Console (see Supplemental Table 5). Statistical differences among multiple groups were analyzed with one-way analysis of variance (ANOVA) test. Significant differences were determined when the P value is less than 0.05. All gene expression data of acute lymphoblastic leukemia (ALL), which derived from B precursor cell, are obtained from Therapeutically Applicable Research to Generate Effective Treatment (TARGET, https://ocg.cancer.gov/programs/target/data-matrix), including Phase I and Phase II (B-ALL) studies of ~200 relapse-enriched cases (patients >9 years old, without BCR/ABL fusion and hypodiploid), with additional 500 precursor B-cell all cases for validation in Phase II study (60, 61). Gene expression data were processed by the Affymetrix U133 Plus 2.0 Array platform. For the correlation between transcriptional expression of IL-21, CD274, CD177, and LY6G6D, we used Spearman's correlation and considered |Rs| >0.2 and FDR <0.05 as significant correlation.

Statistical Analysis. Data were analyzed by Student's two-tailed t-test or one-way ANOVA for multiple comparisons or Mantel-Cox log-rank test for mouse survival using GraphPad Prism 4.0 software (GraphPad Software, La Jolla, CA) and represented as mean ± SEM. Differences were considered significant when P value <0.05. The

correlation of transcriptional expression calculated by Spearman's correlation and considered |R| > 0.2 and FDR < 0.05 as significant correlation.

Study approval. Animal experiments in this study were approved and carried out following the protocol (Protocol #AUP-0115-0005) provided by the Institutional Animal Care and Use Committee (IACUC) at Houston Methodist Research Institute. IACUC uses the National Institute of Health (NIH) Guide for the Care and Use of Laboratory Animals, which is based on the U.S. Government Principles for Utilization and Care of Vertebrate Animals Used in Testing, Research, and Training. The human subject study was performed in accordance with institutional guidelines and the approved protocol (Protocol #IBC00000357) by the Institutional Review Board of Houston Methodist Research Institute.

Data availability. Data support the findings of this study are available from the corresponding author upon reasonable request. Source data for the RNA sequencing have been deposited in the GEO repository with accession code GSE132899.

Author Contributions

R-F.W supervised the entire project. P.T. designed, performed and/or analyzed experiments and data. L.Hz, C.X., J.M., X.Y., M.Z., Y.Z., and H.W. provided intelligent inputs and technical support. L.D., and L.H. performed human patient database analysis. J.Y. provided human patient samples and performed pathological analysis. P.T. and R-F.W. wrote the manuscript.

Supplemental Material

Supplemental material includes 7 Figures and 7 Tables, which can be found with this article online.

References

1.   Lorin S, Hamai A, Mehrpour M, and Codogno P. Autophagy regulation and its role in cancer. *Semin Cancer Biol.* 2013;23(5):361-79.

2.   Deretic V, Saitoh T, and Akira S. Autophagy in infection, inflammation and immunity. *Nat Rev Immunol.* 2013;13(10):722-37.

3.   Qu X, Yu J, Bhagat G, Furuya N, Hibshoosh H, Troxel A, et al. Promotion of tumorigenesis by heterozygous disruption of the beclin 1 autophagy gene. *J Clin Invest.* 2003;112(12):1809-20.

4.   Powell DR, and Huttenlocher A. Neutrophils in the Tumor Microenvironment. *Trends Immunol.* 2016;37(1):41-52.

5.   Zenaro E, Pietronigro E, Della Bianca V, Piacentino G, Marongiu L, Budui S, et al. Neutrophils promote Alzheimer's disease-like pathology and cognitive decline via LFA-1 integrin. *Nat Med.* 2015;21(8):880-6.

6.   Gatjen M, Brand F, Grau M, Gerlach K, Kettritz R, Westermann J, et al. Splenic Marginal Zone Granulocytes Acquire an Accentuated Neutrophil B-Cell Helper

Phenotype in Chronic Lymphocytic Leukemia. *Cancer Res.* 2016;76(18):5253-65.

7.   Sangaletti S, Tripodo C, Vitali C, Portararo P, Guarnotta C, Casalini P, et al. Defective stromal remodeling and neutrophil extracellular traps in lymphoid tissues favor the transition from autoimmunity to lymphoma. *Cancer Discov.* 2014;4(1):110-29.

8.   Puga I, Cols M, Barra CM, He B, Cassis L, Gentile M, et al. B cell-helper neutrophils stimulate the diversification and production of immunoglobulin in the marginal zone of the spleen. *Nat Immunol.* 2011;13(2):170-80.

9.   Sun C, Mezzadra R, and Schumacher TN. Regulation and Function of the PD-L1 Checkpoint. *Immunity.* 2018;48(3):434-52.

10.   Goodman A, Patel SP, and Kurzrock R. PD-1-PD-L1 immune-checkpoint blockade in B-cell lymphomas. *Nat Rev Clin Oncol.* 2017;14(4):203-20.

11.   Pfeiler S, Khandagale AB, Magenau A, Nichols M, Heijnen HF, Rinninger F, et al. Distinct surveillance pathway for immunopathology during acute infection via autophagy and SR-BI. *Sci Rep.* 2016;6:34440.

12.   Mittal M, Siddiqui MR, Tran K, Reddy SP, and Malik AB. Reactive oxygen species in inflammation and tissue injury. *Antioxid Redox Signal.* 2014;20(7):1126-67.

13.   van Rooijen N, Bakker J, and Sanders A. Transient suppression of macrophage functions by liposome-encapsulated drugs. *Trends in biotechnology.* 1997;15(5):178-85.

14.   Vassiloyanakopoulos AP, Okamoto S, and Fierer J. The crucial role of polymorphonuclear leukocytes in resistance to Salmonella dublin infections in genetically susceptible and resistant mice. *Proceedings of the National Academy of Sciences of the United States of America.* 1998;95(13):7676-81.

15.   Li TJ, Jiang YM, Hu YF, Huang L, Yu J, Zhao LY, et al. Interleukin-17-Producing Neutrophils Link Inflammatory Stimuli to Disease Progression by Promoting Angiogenesis in Gastric Cancer. *Clin Cancer Res.* 2017;23(6):1575-85.

16.   Li L, Huang L, Vergis AL, Ye H, Bajwa A, Narayan V, et al. IL-17 produced by neutrophils regulates IFN-gamma-mediated neutrophil migration in mouse kidney ischemia-reperfusion injury. *J Clin Invest.* 2010;120(1):331-42.

17.   Taylor PR, Roy S, Leal SM, Jr., Sun Y, Howell SJ, Cobb BA, et al. Activation of neutrophils by autocrine IL-17A-IL-17RC interactions during fungal infection is regulated by IL-6, IL-23, RORgammat and dectin-2. *Nat Immunol.* 2014;15(2):143-51.

18.   Arthur JS, and Ley SC. Mitogen-activated protein kinases in innate immunity. *Nature reviews Immunology.* 2013;13(9):679-92.

19.   Xu P, Duong DM, Seyfried NT, Cheng D, Xie Y, Robert J, et al. Quantitative proteomics reveals the function of unconventional ubiquitin chains in proteasomal degradation. *Cell.* 2009;137(1):133-45.

20.   Heckl D, Kowalczyk MS, Yudovich D, Belizaire R, Puram RV, McConkey ME, et al. Generation of mouse models of myeloid malignancy with combinatorial genetic lesions using CRISPR-Cas9 genome editing. *Nat Biotechnol.* 2014;32(9):941-6.

21.   Morse HC, 3rd, Anver MR, Fredrickson TN, Haines DC, Harris AW, Harris NL, et al. Bethesda proposals for classification of lymphoid neoplasms in mice. *Blood.* 2002;100(1):246-58.

22.   Stranges PB, Watson J, Cooper CJ, Choisy-Rossi CM, Stonebraker AC, Beighton RA, et al. Elimination of antigen-presenting cells and autoreactive T cells by Fas contributes to prevention of autoimmunity. *Immunity.* 2007;26(5):629-41.

23.   Nie Y, Waite J, Brewer F, Sunshine MJ, Littman DR, and Zou YR. The role of CXCR4 in maintaining peripheral B cell compartments and humoral immunity. *The Journal of experimental medicine.* 2004;200(9):1145-56.

24.   Allende ML, Tuymetova G, Lee BG, Bonifacino E, Wu YP, and Proia RL. S1P1 receptor directs the release of immature B cells from bone marrow into blood. *The Journal of experimental medicine.* 2010;207(5):1113-24.

25.   Somasundaram R, Prasad MA, Ungerback J, and Sigvardsson M. Transcription factor networks in B-cell differentiation link development to acute lymphoid leukemia. *Blood.* 2015;126(2):144-52.

26.   Shojaee S, Chan LN, Buchner M, Cazzaniga V, Cosgun KN, Geng H, et al. PTEN opposes negative selection and enables oncogenic transformation of pre-B cells. *Nat Med.* 2016;22(4):379-87.

27.   Liu H, Zhang H, Wu X, Ma D, Wu J, Wang L, et al. Nuclear cGAS suppresses DNA repair and promotes tumorigenesis. *Nature.* 2018;563(7729):131-6.

28.   Rickert RC. New insights into pre-BCR and BCR signalling with relevance to B cell malignancies. *Nat Rev Immunol.* 2013;13(8):578-91.

29.   Yu H, Pardoll D, and Jove R. STATs in cancer inflammation and immunity: a leading role for STAT3. *Nat Rev Cancer.* 2009;9(11):798-809.

30.   Malin S, McManus S, Cobaleda C, Novatchkova M, Delogu A, Bouillet P, et al. Role of STAT5 in controlling cell survival and immunoglobulin gene

recombination during pro-B cell development. *Nature immunology.* 2010;11(2):171-9.

31.   Jarosinski KW, and Massa PT. Interferon regulatory factor-1 is required for interferon-gamma-induced MHC class I genes in astrocytes. *J Neuroimmunol.* 2002;122(1-2):74-84.

32.   Garcia-Diaz A, Shin DS, Moreno BH, Saco J, Escuin-Ordinas H, Rodriguez GA, et al. Interferon Receptor Signaling Pathways Regulating PD-L1 and PD-L2 Expression. *Cell Rep.* 2017;19(6):1189-201.

33.   Coelho MA, de Carne Trecesson S, Rana S, Zecchin D, Moore C, Molina-Arcas M, et al. Oncogenic RAS Signaling Promotes Tumor Immunoresistance by Stabilizing PD-L1 mRNA. *Immunity.* 2017;47(6):1083-99 e6.

34.   Mezzadra R, Sun C, Jae LT, Gomez-Eerland R, de Vries E, Wu W, et al. Identification of CMTM6 and CMTM4 as PD-L1 protein regulators. *Nature.* 2017;549(7670):106-10.

35.   Loughner CL, Bruford EA, McAndrews MS, Delp EE, Swamynathan S, and Swamynathan SK. Organization, evolution and functions of the human and mouse Ly6/uPAR family genes. *Hum Genomics.* 2016;10:10.

36.   Lee PY, Wang JX, Parisini E, Dascher CC, and Nigrovic PA. Ly6 family proteins in neutrophil biology. *J Leukoc Biol.* 2013;94(4):585-94.

37.   Martinez J, Malireddi RK, Lu Q, Cunha LD, Pelletier S, Gingras S, et al. Molecular characterization of LC3-associated phagocytosis reveals distinct roles for Rubicon, NOX2 and autophagy proteins. *Nat Cell Biol.* 2015;17(7):893-906.

38.   Gutierrez MG, Master SS, Singh SB, Taylor GA, Colombo MI, and Deretic V. Autophagy is a defense mechanism inhibiting BCG and Mycobacterium tuberculosis survival in infected macrophages. *Cell.* 2004;119(6):753-66.

39.   Baldassare JJ, Bi Y, and Bellone CJ. The role of p38 mitogen-activated protein kinase in IL-1 beta transcription. *J Immunol.* 1999;162(9):5367-73.

40.   Noubade R, Krementsov DN, Del Rio R, Thornton T, Nagaleekar V, Saligrama N, et al. Activation of p38 MAPK in CD4 T cells controls IL-17 production and autoimmune encephalomyelitis. *Blood.* 2011;118(12):3290-300.

41.   Greten FR, Arkan MC, Bollrath J, Hsu LC, Goode J, Miething C, et al. NF-kappaB is a negative regulator of IL-1beta secretion as revealed by genetic and pharmacological inhibition of IKKbeta. *Cell.* 2007;130(5):918-31.

42.   Hsu LC, Enzler T, Seita J, Timmer AM, Lee CY, Lai TY, et al. IL-1beta-driven neutrophilia preserves antibacterial defense in the absence of the kinase IKKbeta. *Nat Immunol.* 2011;12(2):144-50.

43. Aras S, and Zaidi MR. TAMeless traitors: macrophages in cancer progression and metastasis. *Br J Cancer.* 2017;117(11):1583-91.

44. Mueller SN, and Germain RN. Stromal cell contributions to the homeostasis and functionality of the immune system. *Nature reviews Immunology.* 2009;9(9):618-29.

45. Hendriks RW, Yuvaraj S, and Kil LP. Targeting Bruton's tyrosine kinase in B cell malignancies. *Nature reviews Cancer.* 2014;14(4):219-32.

46. Beck TC, Gomes AC, Cyster JG, and Pereira JP. CXCR4 and a cell-extrinsic mechanism control immature B lymphocyte egress from bone marrow. *The Journal of experimental medicine.* 2014;211(13):2567-81.

47. Cyster JG, and Schwab SR. Sphingosine-1-phosphate and lymphocyte egress from lymphoid organs. *Annual review of immunology.* 2012;30:69-94.

48. Le Y, Zhu BM, Harley B, Park SY, Kobayashi T, Manis JP, et al. SOCS3 protein developmentally regulates the chemokine receptor CXCR4-FAK signaling pathway during B lymphopoiesis. *Immunity.* 2007;27(5):811-23.

49. Yoshida N, Kitayama D, Arima M, Sakamoto A, Inamine A, Watanabe-Takano H, et al. CXCR4 expression on activated B cells is downregulated by CD63 and IL-21. *J Immunol.* 2011;186(5):2800-8.

50. Bubier JA, Sproule TJ, Foreman O, Spolski R, Shaffer DJ, Morse HC, 3rd, et al. A critical role for IL-21 receptor signaling in the pathogenesis of systemic lupus erythematosus in BXSB-Yaa mice. *Proc Natl Acad Sci U S A.* 2009;106(5):1518-23.

51. Stolfi C, Pallone F, Macdonald TT, and Monteleone G. Interleukin-21 in cancer immunotherapy: Friend or foe? *Oncoimmunology.* 2012;1(3):351-4.

52. Ware CF. APRIL and BAFF connect autoimmunity and cancer. *J Exp Med.* 2000;192(11):F35-8.

53. Scott DW, and Gascoyne RD. The tumour microenvironment in B cell lymphomas. *Nat Rev Cancer.* 2014;14(8):517-34.

54. Leonard WJ, and Wan CK. IL-21 Signaling in Immunity. *F1000Res.* 2016;5.

55. Kinter AL, Godbout EJ, McNally JP, Sereti I, Roby GA, O'Shea MA, et al. The common gamma-chain cytokines IL-2, IL-7, IL-15, and IL-21 induce the expression of programmed death-1 and its ligands. *J Immunol.* 2008;181(10):6738-46.

56.   Zou W, Wolchok JD, and Chen L. PD-L1 (B7-H1) and PD-1 pathway blockade for cancer therapy: Mechanisms, response biomarkers, and combinations. *Sci Transl Med.* 2016;8(328):328rv4.

57.   Shalapour S, Lin XJ, Bastian IN, Brain J, Burt AD, Aksenov AA, et al. Inflammation-induced IgA+ cells dismantle anti-liver cancer immunity. *Nature.* 2017;551(7680):340-5.

58.   Trapnell C, Pachter L, and Salzberg SL. TopHat: discovering splice junctions with RNA-Seq. *Bioinformatics.* 2009;25(9):1105-11.

59.   Subramanian A, Tamayo P, Mootha VK, Mukherjee S, Ebert BL, Gillette MA, et al. Gene set enrichment analysis: a knowledge-based approach for interpreting genome-wide expression profiles. *Proc Natl Acad Sci U S A.* 2005;102(43):15545-50.

60.   Loh ML, Zhang J, Harvey RC, Roberts K, Payne-Turner D, Kang H, et al. Tyrosine kinome sequencing of pediatric acute lymphoblastic leukemia: a report from the Children's Oncology Group TARGET Project. *Blood.* 2013;121(3):485-8.

61.   Ma X, Edmonson M, Yergeau D, Muzny DM, Hampton OA, Rusch M, et al. Rise and fall of subclones from diagnosis to relapse in pediatric B-acute lymphoblastic leukaemia. *Nat Commun.* 2015;6:6604.

Figures and Figure legends
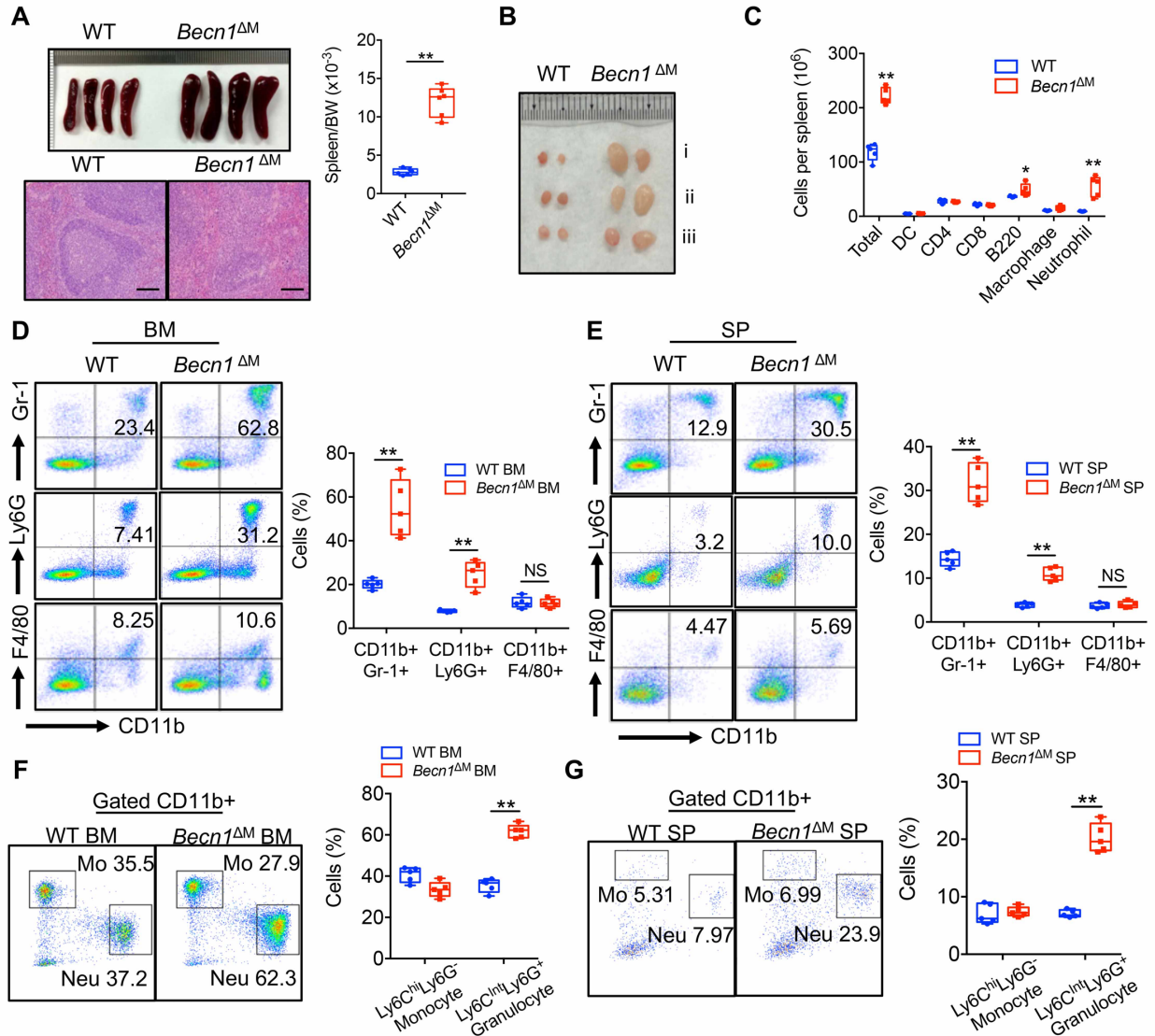
Figure 1. Characterization and phenotypic analysis of *Becn1*ΔM mice.

(**A**) Spleen size comparison between WT and *Becn1*ΔM mice and spleen/ body weight ratio (n=4). H&E staining of spleen sections from WT and *Becn1*ΔM mice. Scale bars, 500 µm.

(**B**) Lymphadenopathy in *Becn1*$^{\Delta M}$ mice compared with WT control, Inguinal (i), axillary (ii), and mesenteric (iii) LNs were examined. Data are representative of 3 independent experiments with 6- to 8-week-old mice (n = 2) in each group.

(**C**) Total number of splenic CD45$^+$CD11c$^+$ DCs, CD4$^+$ T cells, CD8$^+$ T cells, B220$^+$ B cells, CD11b$^+$F4/80$^+$ macrophages, CD11b$^+$Ly6G$^+$ neutrophils from WT and *Becn1*$^{\Delta M}$ mice (n=4).

(**D** and **E**) Representative flow cytometry plots and statistical analysis of Gr-1$^+$CD11b$^+$ myeloid cells, Ly6G$^+$CD11b$^+$ neutrophils and F4/80$^+$CD11b$^+$ macrophage in bone marrow (BM) (D) and spleen (SP) (E) of WT and *Becn1*$^{\Delta M}$ mice (n=5).

(**F** and **G**) Representative flow cytometry plots and statistical analysis of monocytic (Ly6C^{hi}Ly6G$^-$) and granulocytic (Ly6C^{int}Ly6G$^+$) cells in BM (F) and spleen (G) of 6-to 8-week-old WT and *Becn1*$^{\Delta M}$ mice (n=5).

Data shown in panel (**A, C**-**G**) were performed in 6- to 8-week-old mice, presented as boxplots, line represents median with error bars show the mean ± SEM. Statistical between groups calculated using Students' unpaired t-test with significance indicated (*P <0.05, **P <0.01, NS, not significant).
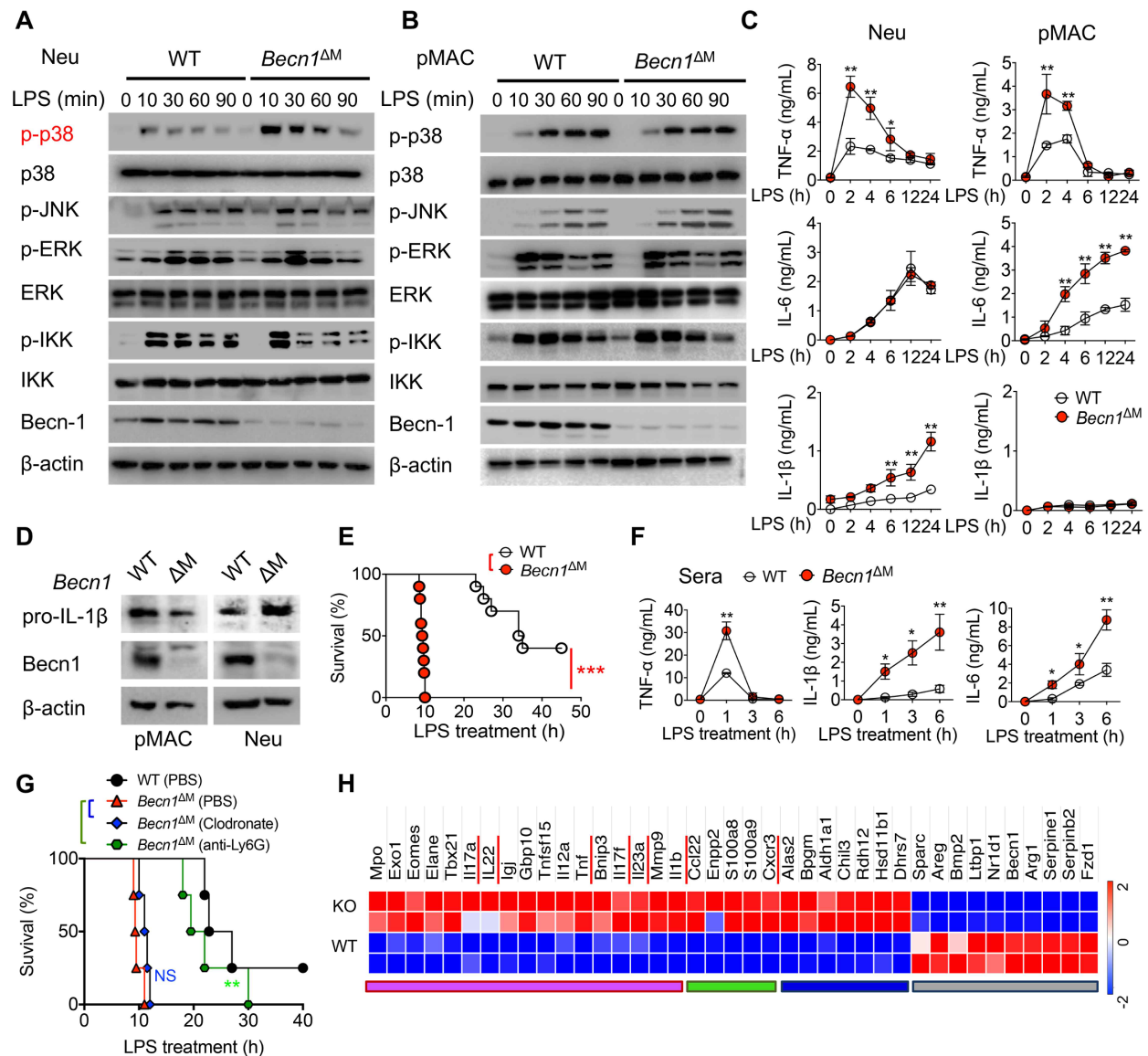
Figure 2. Cell-type-specific regulation of Becn1 in proinflammatory signaling pathways and immune responses.

(**A** and **B**) Neu (A) or pMAC (B) from the periphery of WT and *Becn1*$^{\Delta M}$ mice were treated with LPS for the indicated time points, followed by IB with indicated antibody.

(**C**) ELISA measurement of TNF-α, IL-6 and IL-1β production by Neu and pMAC of WT and *Becn1*$^{\Delta M}$ mice treated with100 ng/ml LPS for indicated time points (n=4).

(**D**) IB of pro-IL-1β expression in Neu or pMAC from WT and *Becn1*$^{\Delta M}$ mice.

(**E**) Survival of WT and *Becn1*$^{\Delta M}$ mice (n = 10; female) treated with high-dose LPS (30 mg/kg, i.p.).

(**F**) Plasma concentrations of TNF-α, IL-6, and IL-1β in WT or *Becn1*$^{\Delta M}$ mice (n=5) at indicated time points after LPS treatment.

(**G**) Survival of WT and *Becn1*$^{\Delta M}$ mice (n = 4; female) treated with PBS- or clodronate-containing liposomes to deplete macrophages or with anti-Ly6G antibody (1A8) to deplete neutrophils, followed by high-dose LPS treatment.

(**H**) Heatmap representation of differential expressed genes in neutrophils isolated from *Becn1*$^{\Delta M}$ mice compared to WT controls: neutrophil-mediated immunity and IL17-related cytokines (purple)*,* chemokine receptor and neutrophil-chemotaxis (green), cell metabolism (blue).

Data in (**A**, **B**, **D**) are representative of 3 independent experiments with 6- to 8-week-old mice (n = 3; female) in each group. Statistical between groups calculated using Students' unpaired t-test as mean ± SEM (**C, F**) and Mantel-Cox log-rank test (**E**, **G**) with significance indicated (*P <0.05, **P <0.01, ***P <0.001, NS, not significant).
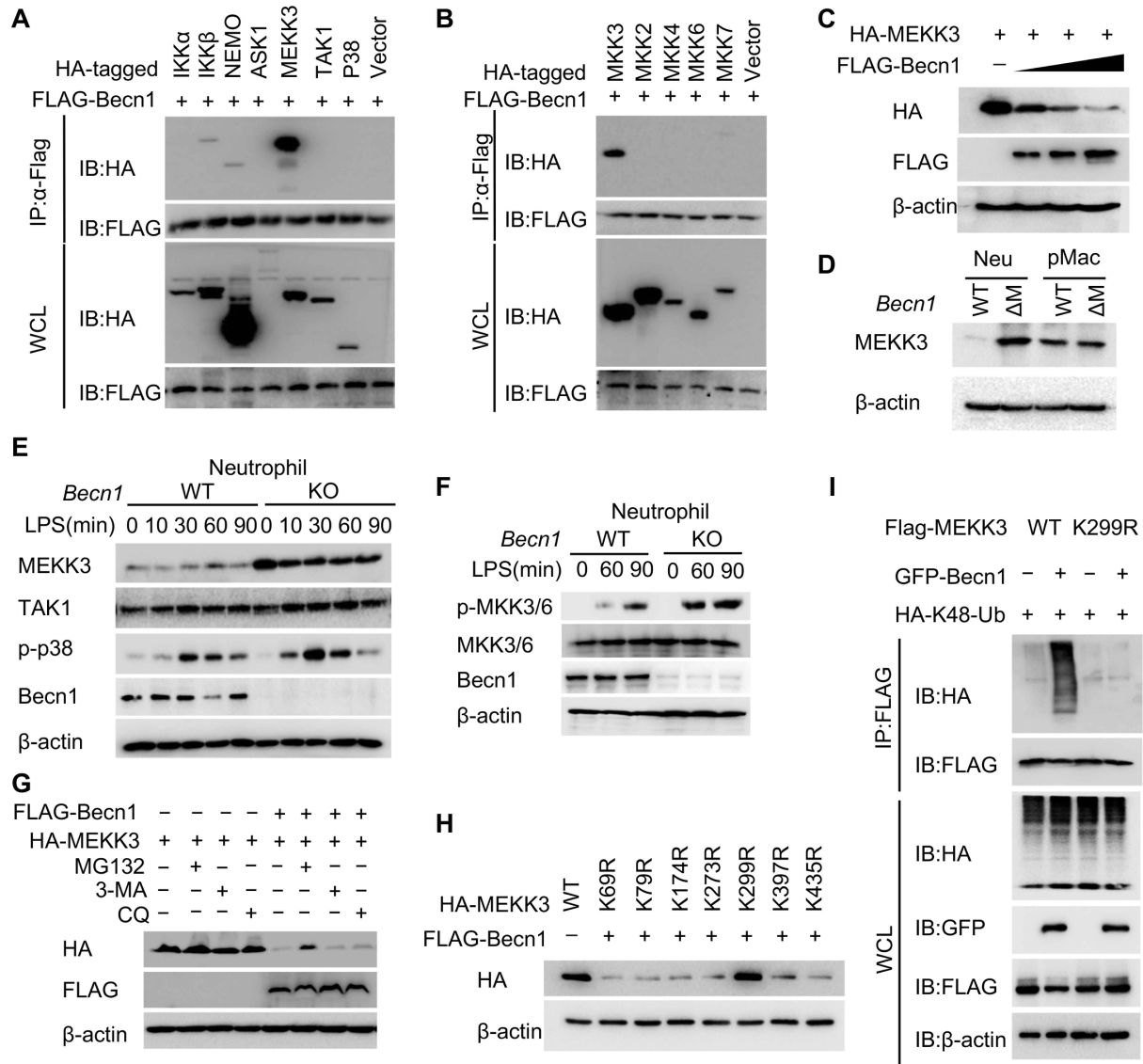
Figure 3. *Becn1* **ablation suppresses proteasomal degradation of neutrophil MEKK3 upstream of p38.**

(**A** and **B**) Screening of Becn1 binding proteins in NF-κB and MAPK pathways in 293T cells. WCL, whole-cell lysate.

(**C**) 293T cells transfected with 100 ng HA-MEKK3 along with increased amount (0, 100, 250, and 500 ng) of FLAG-Becn1, followed by IB with indicated antibody.

(**D**) IB of MEKK3 protein expression in *Becn1*-deficient Neu and pMAC compared to WT controls.

(**E and F**) WT or *Becn1*-deficient neutrophils were treated with LPS for the indicated time points, followed by IB with the antibody against MEKK3, TAK1 or p-p38 (E) and MKK3/6 signaling (F).

(**G**) IB of 293T cells transfected with HA-MEKK3 along with empty vector or FLAG-Becn1 left untreated or treated with proteasome inhibitor MG132 (1 μM) or autophagy inhibitors 3-MA (5 mM) or chloroquine (CQ, 10 μM).

(**H**) IB of 293T cells transfected with WT or HA-MEKK3 (K69R, K79R, K174R, K273R, K299R, K397R, K435R) along with empty vector or FLAG-Becn1.

(**I**) 293T cells were transfected with FLAG-MEKK3 WT or FLAG-MEKK3 K299R along with GFP-Becn1 and HA-Ubiquitin K48 expression vectors, followed by immunoprecipitation with FLAG-beads and IB with indicated antibodies.

Data are representative of 3 independent experiments in 293T cells (**A**-**C**, **G-I**), and with 6- to 8-week old mice (n = 3; female) (**D**-**F**).
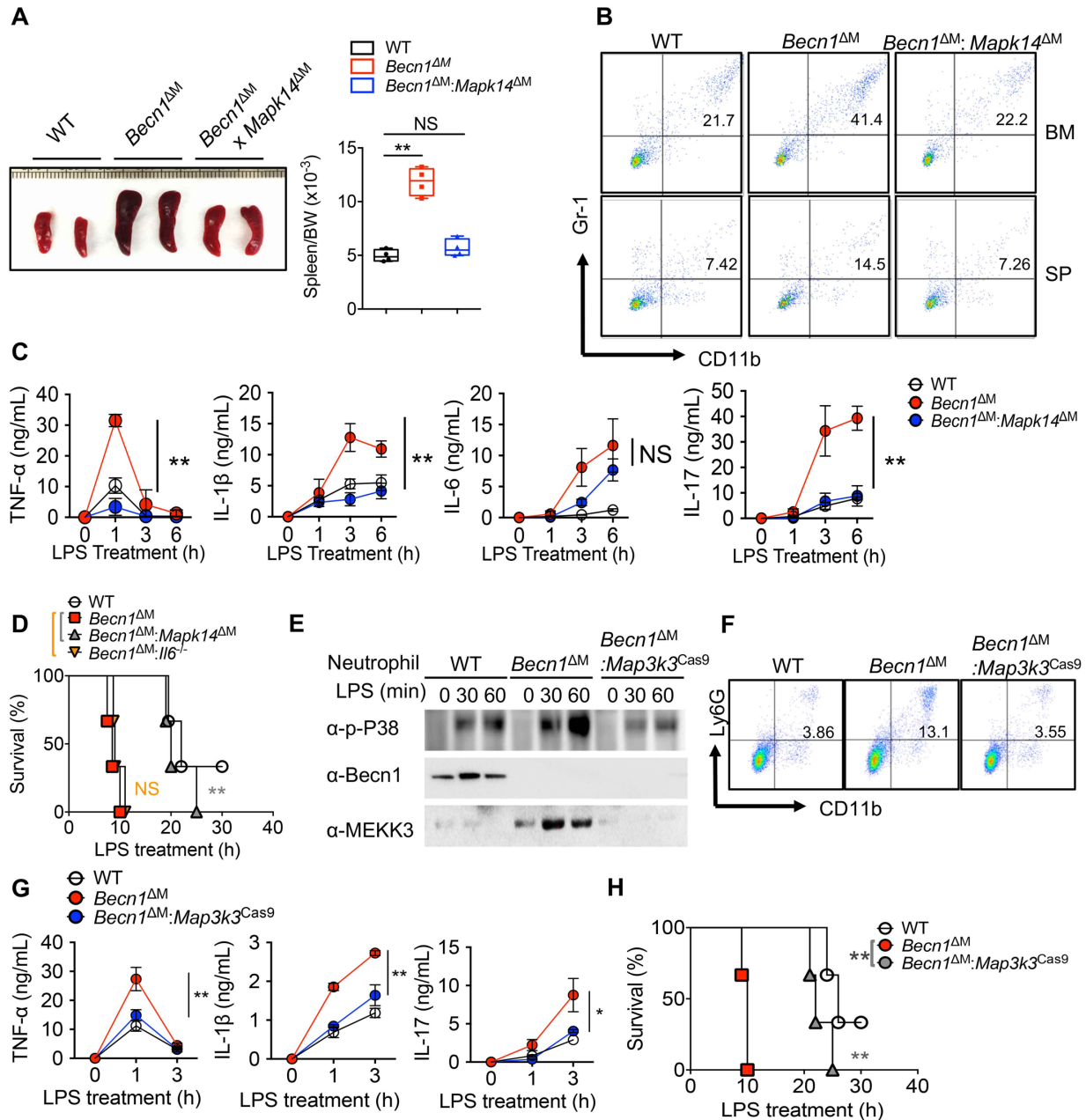
Figure 4. p38 or MEKK3 ablation restores *Becn1^ΔM* mouse phenotype similar to WT.

(**A**) Spleen size (left) and spleen:body weight ratio(right) isolated from WT, *Becn1^ΔM* and *Becn1^ΔM:Mapk14^ΔM* mice (n=4).

(**B**) Representative flow cytometry plots of Gr-1^+CD11b^+ neutrophils in WT, *Becn1^ΔM* and *Becn1^ΔM:Mapk14^ΔM* mice.

(**C**) ELISA measurement of TNF-α, IL-6, IL-1β and IL-17A production in serum from WT, *Becn1$^{\Delta M}$* and *Becn1$^{\Delta M}$:Mapk14$^{\Delta M}$* mice treated with high-dose LPS.

(**D**) Survival of WT, *Becn1$^{\Delta M}$*, *Becn1$^{\Delta M}$:Mapk14$^{\Delta M}$* and *Becn1$^{\Delta M}$:Il6$^{-/-}$* mice treated with high-dose LPS.

(**E**) Neutrophils isolated from WT, *Becn1$^{\Delta M}$* and *Becn1$^{\Delta M}$:Map3k3^{Cas9}* mice treated with LPS for the indicated time points, followed by IB with indicated antibody.

(**F**) Representative flow cytometry plots of CD11b$^+$Ly6G$^+$ neutrophils in WT, *Becn1$^{\Delta M}$* and *Becn1$^{\Delta M}$:Map3k3^{Cas9}* mice.

(**G**) ELISA analysis of TNF-α, IL-1β, and IL-17A production in serum from WT, *Becn1$^{\Delta M}$* and *Becn1$^{\Delta M}$:Map3k3^{Cas9}* mice treated with high-dose LPS.

(**H**) Survival of WT, *Becn1$^{\Delta M}$* and *Becn1$^{\Delta M}$:Map3k3^{Cas9}* mice treated with high-dose LPS. Data are representative of 3 independent experiments with 6- to 8-week-old mice (n=3; female) (**B**-**D**) and 10- to 12-week-old mice (n=3; female) (**E**-**G**). Statistical between groups calculated using one-way ANOVA with Dunnett's multiple comparison test (**A, C**, **G**) and Mantel-Cox log-rank test (**D**, **H**) with significance indicated (*P <0.05, **P <0.01, NS, not significant).
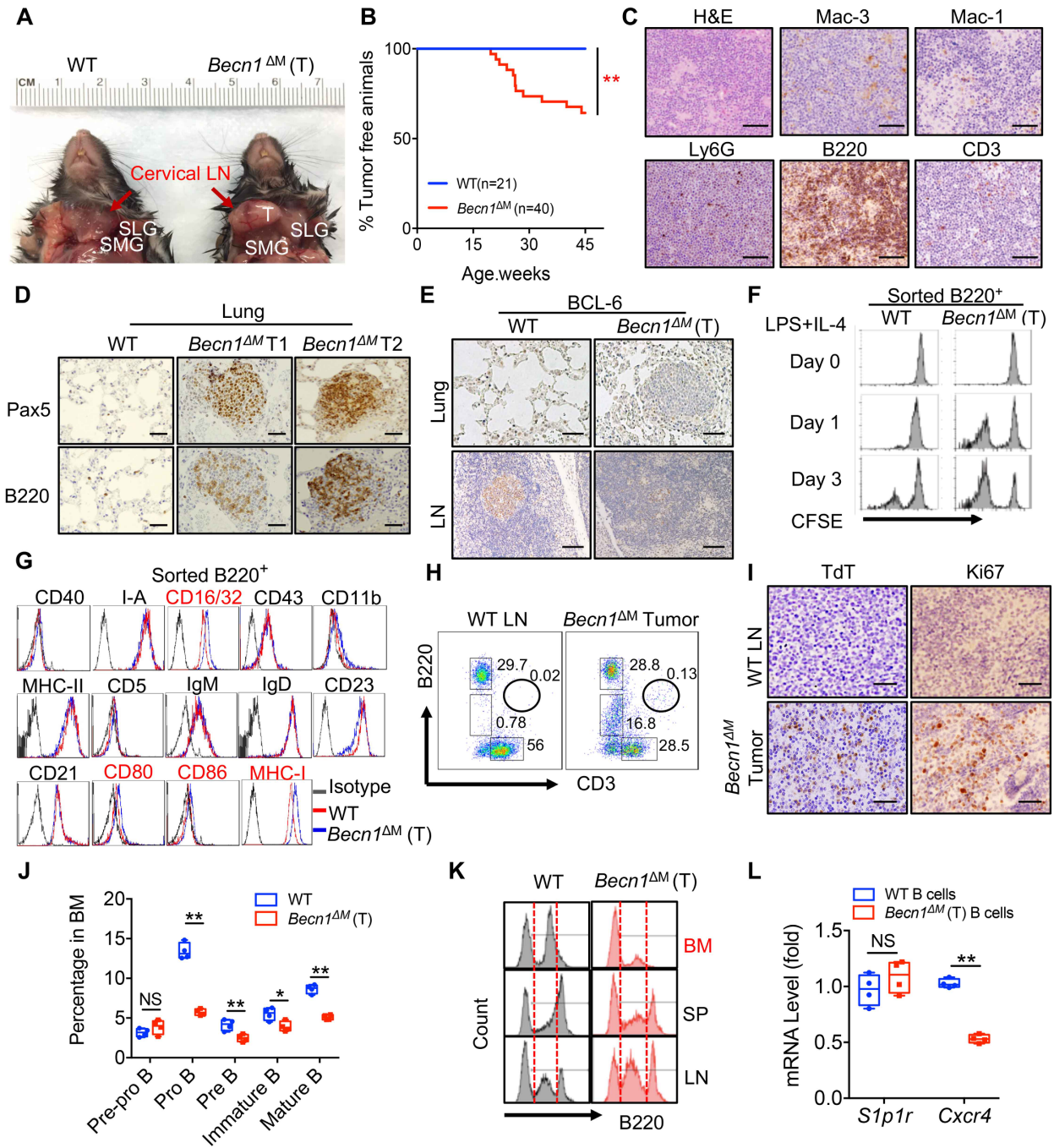
Figure 5. Identification of MHC-I^{hi}B220^{lo} TdT$^+$ pre-B cell lymphoma in *Becn1*$^{\Delta M}$ mice.

(**A**) Tumor formation in cervical LN (red arrows) in *Becn1*$^{\Delta M}$ mice. T, tumor; SLG, sublingual gland; SMG, submandibular gland.

(**B**) Kaplan-Meier curves for tumor-free animals were calculated based on the tumor latency of the control (n=21; 11 females, 10 males; blue) and *Becn1*$^{\Delta M}$ mice (n=40; 31 females, 9 males; red).

(**C**) IHC staining of tumor sections from *Becn1*$^{\Delta M}$ tumor-bearing mice with indicated antibody. Scale bars, 500 μm.

(**D**) IHC staining of lung sections stained with B cell markers. T1, low antibody concentration, T2, high antibody concentration. Scale bars, 100 μm.

(**E**) IHC staining of lung sections stained with anti-Bcl-6 (LN follicular B cells as a positive control). Scale bars, 100 μm.

(**F**) FACS analysis of CFSE-labeled (APC-CFSE) B cells treated with LPS and IL-4 at indicated time points.

(**G**) FACS analysis of B cell surface markers. Significant right-shift markers were indicated in red.

(**H**) FACS analysis of cell populations in tumor with indicated antibody.

(**I**) IHC staining of tumor sections with TdT and Ki67 antibodies. Scale bars, 100 μm.

(**J**) FACS and statistical analysis of BM pre-pro B (B220$^+$CD43$^+$), pro B (B220$^+$CD43^{lo}), pre B (B220$^+$CD43$^-$), immature B (B220$^+$CD43$^-$IgM$^+$IgD$^-$) and mature B (B220$^+$CD43$^-$IgM$^+$IgD$^+$) populations.

(**K**) FACS analysis of B220$^+$ B cells population in BM, SP, and LN of WT and *Becn1*$^{\Delta M}$ tumor-bearing mice.

(**L**) qRT-PCR of *S1p1r* and *Cxcr4* mRNA in B220$^+$ cells from WT (n=5) and *Becn1*$^{\Delta M}$ tumor-bearing mice (n=9).

Data are presented as boxplots with error bars show the mean ± SEM (**J** and **L**), and are representative of 3 independent experiments (n = 3; female) (**A**, **C-I**, **K**). Statistical between groups calculated using Mantel-Cox log-rank test (**B**), Students' unpaired t-test (**J**, **L**) with significance indicated (*P <0.05, **P <0.01, NS, not significant).
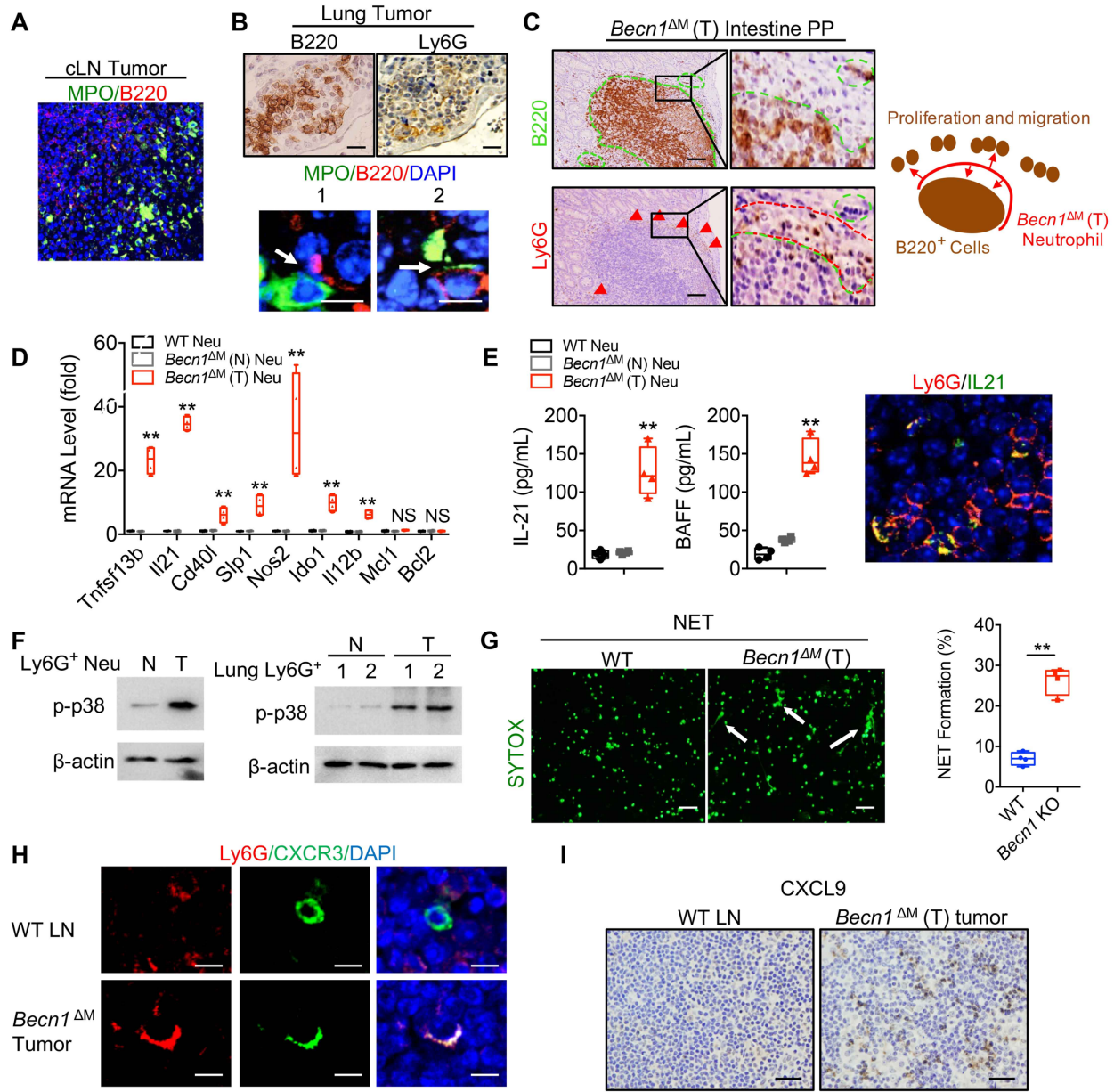
Figure 6. *Becn1* deficiency induces B cell helper pro-tumorigenic function of neutrophils.

(**A** and **B**) IHC staining or IF of tumor in cLN and lung stained with indicated antibody showing the interaction of B cells with neutrophils. DAPI, DNA-intercalating dye (nucleus, blue). Scale bars, 25 µm.

(**C**) IHC staining of intestinal payer's patches sections with indicated antibody. Scale bars, 500 μm. Cartoon illustrates a strip of neutrophils surround at the edge of B cell zone likely to support B cell proliferation and migration.

(**D**) qRT-PCR of B cell helper neutrophil signature genes.

(**E**) ELISA analysis of BAFF and IL-21 production by neutrophils after *in vitro* culture for 12 h. IF showed accumulation of Gr-1$^+$CD11b$^+$ neutrophils in the tumor expressing IL-21.

(**F**) IB of p38 activation in neutrophils from lymphoma (T) and lungs in *Becn1*$^{\Delta M}$ tumor-bearing mice compared to WT controls (N, normal).

(**G**) Fluorescence and statistical analysis of NETs formation in neutrophils by using SYTOX dye (green). White arrows indicate NETs. Scale bars, 100 μm.

(**H**) IF of tumor section with Ly6G (red) and CXCR3 (green) antibody compared to WT LN. Scale bars, 25 μm.

(**I**) IHC staining of tumor sections with anti-CXCL9 antibody compared to WT LN. Scale bars, 200 μm.

Data are presented as boxplots with error bars show the mean ± SEM (**D, E, G**), and are representative of 3 independent experiments (n = 3; female) (**A-C**, **F**, **H**, **I**). Statistical between groups calculated using one-way ANOVA with Dunnett's multiple comparison test (**D, E**), Students' unpaired t-test (**G**) with significance indicated (*P <0.05, **P <0.01, NS, not significant).
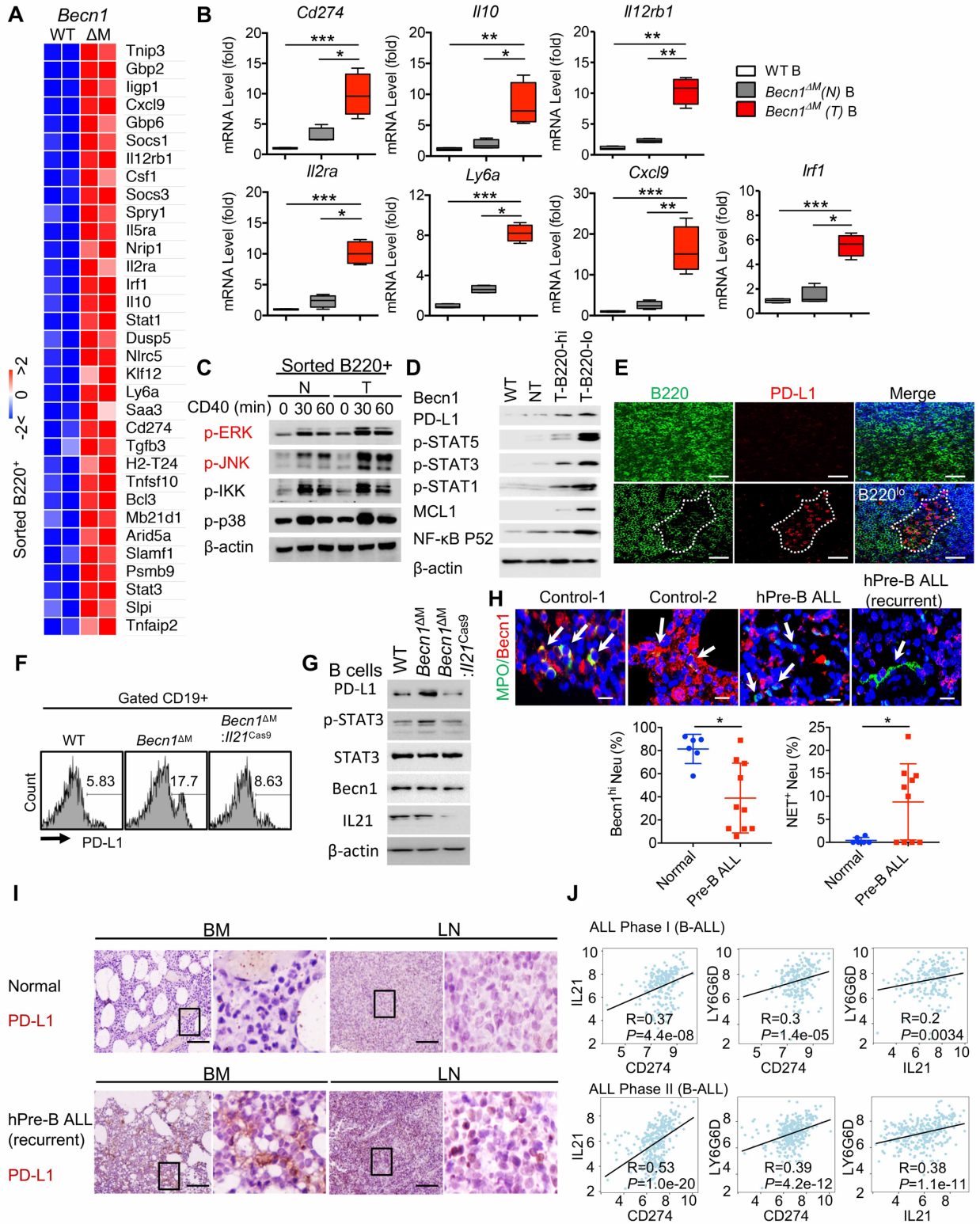
Figure 7. Neutrophil Becn1 level correlates with PD-L1 in pre-B lymphoma.

(**A** and **B**) Heatmap of upregulated genes in B cells with selected genes confirmed by qRT-PCR (n=4).

(**C**) IB of B220$^+$ cells with indicated antibody after stimulation with CD40 agonist.

(**D**) IB of B cells with indicated antibody comparing B220^{hi} vs. B220^{lo} cells in tumor.

(**E**) IF of tumor sections with anti-PD-L1 (red) and anti-B220 (green). Scale bars, 100 μm.

(**F**) FACS analysis of PD-L1 expression in B cells from WT, *Becn1*$^{\Delta M}$ (T) and *Becn1*$^{\Delta M}$: *Il21*^{Cas9} DKO mice.

(**G**) Immunoblot analysis of B cells from WT, *Becn1*$^{\Delta M}$ (T) and *Becn1*$^{\Delta M}$: *Il21*^{Cas9} DKO mice with indicated antibodies.

(**H**) IF and statistical analysis of Becn1 expression in MPO$^+$ cells with or without NET-formation in pre-B-ALL compared to normal controls. Scale bars, 25 μm. (normal, n=6; pre-B ALL, n=10).

(**I**) IHC of PD-L1 expression in pre-ALL samples (n=10) compared to normal controls (n=6). Scale bars, 100 μm. LN, reactive lymphoid hyperplasia,

(**J**) Correlation of IL-21, PD-L1 and neutrophil marker (LY6G6D) in B-ALL dataset (TARGET).

Data are presented as boxplots with error bars show the mean ± SEM (**B**, **H**), and are representative of 3 independent experiments (n = 3; female) (**C**-**G**). Statistical analysis using one-way ANOVA with Dunnett's multiple comparison test (**B**), Students' unpaired t-test (**H**) with significance indicated (*P <0.05, **P <0.01, ***P <0.001, NS, not significant).